EXPERIMENTAL STUDY OF THE PVTX PROPERTIES IN PART OF THE TERNARY SYSTEM H_2O-NaCl-CO_2

by

Christian Schmidt

Dissertation submitted to the Faculty of the

Virginia Polytechnic Institute and State University

in partial fulfillment of the requirements for the degree of

DOCTOR OF PHILOSOPHY

in

Geological Sciences

APPROVED: _____
R. J. Bodnar, Chairman

_____ _____
I-M. Chou **E. Roedder**

_____ _____
R. J. Tracy **J. R. Craig**

March 21, 1997
Blacksburg, Virginia

Key Words: Water - Sodium Chloride - Carbon Dioxide, PVTX Properties, Synthetic Fluid Inclusions, Raman Spectroscopy, Hydrothermal Diamond-Anvil Cell

EXPERIMENTAL STUDY OF THE PVTX PROPERTIES IN PART OF THE TERNARY SYSTEM H_2O-NaCl-CO_2

by

Christian Schmidt

(ABSTRACT)

Phase equilibria and volumetric properties in the system H_2O-NaCl-CO_2 were determined experimentally for pressures between about 1 to 6 kbar, temperatures of 300° to 800°C, and fluid compositions up to 40 wt% NaCl and 20 mol% CO_2, both relative to water. This was accomplished by using the synthetic fluid inclusion technique in conjunction with conventional microthermometry, a hydrothermal diamond-anvil cell and Raman spectroscopy.

At constant salinity, the high-pressure portion of the solvus migrates to higher pressures and temperatures with increasing CO_2 concentration. Immiscibility is possible in this ternary system over almost the entire range of crustal P-T conditions at salinities equal to or in excess of 20 wt% NaCl and carbon dioxide concentrations between about 30 and 70 mol% CO_2. The dP/dT slopes of lines of equal homogenization temperature decrease nonlinearly with increasing homogenization temperature; at constant homogenization temperature, these slopes become steeper (higher) along pseudobinaries with addition of carbon dioxide and particularly with addition of NaCl. Up to concentrations of 20 wt% NaCl and 20 mol% CO_2, a sharp rise in the critical temperature was observed with increasing salinity at a fixed H_2O/CO_2 ratio. The critical point shifts rapidly towards higher pressures with increasing carbon dioxide concentration. Addition of carbon dioxide to an aqueous 40 wt% NaCl solution results in a slight elevation of the halite dissolution temperature under vapor-saturated conditions.

A significant error can be associated with the calculation of molar volumes from measured densities of the carbonic phase of H_2O-NaCl-CO_2 inclusions. To avoid such errors, phase diagrams were constructed based on the obtained lines of equal homogenization temperature for salinities between 6 and 40 wt% NaCl and carbon dioxide concentrations between 5 and 20 mol% relative to water. These diagrams are of direct applicability to the interpretation of natural fluid inclusions from a wide variety of geologic environments.

ACKNOWLEDGMENTS

The research presented here could not have been accomplished without the funding, guidance, help, and encouragement of Bob Bodnar, who was instrumental in my development as a student and scientist; I was lucky to have him as advisor. I am grateful to I-Ming Chou and Bill Bassett who made the analysis of synthetic fluid inclusions using a hydrothermal diamond-anvil cell possible, and look forward to continued collaboration. I would also like to thank Ed Roedder, Bob Tracy, and Jim Craig for their interest, advice, and willingness to serve as committee members. The support and contributions to various aspects of this study by Sarah Beutner, Mark Fortney, Frank Harrison, David Hewitt, John Mavrogenes, Don Rimstidt, Kevin Rosso, and James Student are greatly appreciated. Many thanks to the friendly and helpful staff and my fellow graduate students at the geology department of Virginia Tech; I consider myself fortunate to have worked with such a fine group. Last but not least, I particularly would like to thank all the friends I made during my stay here and my folks and friends back in Germany for their support and encouragement.

TABLE OF CONTENTS

LIST OF FIGURES

INTRODUCTION

With the increased application of fluid inclusions in mineralogy and petrology in the last four decades, it became evident that the composition of many inclusions from a variety of crustal environments can be adequately represented by the ternary system H_2O-NaCl-CO_2. The presence of such fluids was observed in contact metamorphic, greenschist, and amphibolite facies rocks, granitoids, pegmatites, alkaline igneous rocks, carbonatites, geothermal brines and a wide variety of hydrothermal deposits (Roedder, 1984; Labotka, 1991). Two properties of the system, (1) extension of conditions of immiscibility to higher pressures and temperatures (compared to either of the binary systems H_2O-NaCl and H_2O-CO_2) and (2) the change in the temperature and pressure at which a given set of minerals will be in equilibrium due to lowering of the water activity by the addition of both an electrolyte and a nonpolar volatile component (Bowers and Helgeson, 1983a, b), have substantial petrologic and geochemical implications, which triggered a number of experimental studies on solubilities, phase equilibria, and PVTX properties.

Critical properties, solvus location, and salt solubility in the fluid phase of water-volatile-electrolyte systems are the subjects of current research related to supercritical water oxidation technology for the treatment of hazardous organic wastes. These data are needed to optimize operating conditions of supercritical water oxidation reactors and the design of salt separation loops (Shaw et al., 1991; Tester et al., 1992; Bodnar, 1995). Phase equilibrium data for the H_2O-NaCl-CO_2 system are also relevant to the desalination of seawater (Bozzo et al., 1975) and storage of nuclear waste in evaporites (Roedder, 1984 and references therein).

Determination of the solubility of CO_2 in H_2O-NaCl mixtures was the main goal of early work conducted in this ternary system. Ellis and Golding (1963) determined the solubility of CO_2 in sodium chloride solutions up to 2 molal NaCl and 330°C. Takenouchi and Kennedy (1965) extended these data to 20 wt%* NaCl, 1.4 kbar, and 450°C. Drummond (1981) studied CO_2 solubility in NaCl solutions up to 6 molal between 25°C and 400°C. Malinin and Savelyeva (1972), Malinin and Kurovskaya (1975), and Yasunishi and Yoshida (1979) determined carbon dioxide solubilities in aqueous sodium chloride solutions up to 6 molal and at temperatures between 15°C and 150°C. These studies show that addition of NaCl results in a significant reduction of CO_2 solubility ("salting-out" effect).

Compared to phase equilibrium data, volumetric data for the H_2O-NaCl-CO_2 system were less common until relatively recently. The synthetic fluid inclusion technique was used to determine solvus locations and lines of constant homogenization temperatures (Kotelnikov and Kotelnikova, 1990; Frantz et al., 1992; Johnson, 1991 and 1992; Shmulovich and Plyasunova, 1993; Schmidt et al., 1995). Joyce and Holloway (1993) and Blencoe et al. (1996) obtained activity-mole fraction relations of water in H_2O-CO_2-NaCl mixtures directly by reacting fluid samples in an internally-heated pressure vessel at constant pressure, temperature, and hydrogen fugacity and measuring the shift in mole fraction H_2O after quenching. Volumetric data for compositions above 20 wt% NaCl are scarce. PTX conditions of critical points are only known for limited ranges along the binary joins H_2O-NaCl and H_2O-CO_2 (Sourirajan and Kennedy 1962; Tödheide and Franck, 1963; Takenouchi and Kennedy, 1964; Knight and Bodnar 1989; Sterner and Bodnar, 1991). The most extensive experimental dataset was obtained by Gehrig (1980) for molar volumes and immiscibility limits along the (H_2O + 6, 10, and 20 wt% NaCl) - CO_2 pseudobinaries up to 3 kbar and temperatures to 560°C using a

* Throughout text, figures, and tables, concentrations are given as wt% or mol% of a substance relative to water, e.g. 20 wt% NaCl = (20 g NaCl * 100%)/(20 g NaCl + 80 g H_2O). The sodium chloride and carbon dioxide concentrations do **not** refer to a bulk composition in a ternary H_2O-NaCl-CO_2 mixture.

high-pressure variable-volume autoclave. These data are also the main empirical basis of the modified Redlich-Kwong equation of state by Bowers and Helgeson (1983a) and the equation of state of Duan et al. (1995), which uses the approach of Anderko and Pitzer (1993). Brown and Lamb (1989) modeled isochore positions of H_2O-NaCl-CO_2 mixtures by linear interpolation of H_2O-NaCl and CO_2 isochores.

Low-temperature phase equilibria involving clathrate were studied by Bozzo et al. (1975) and Diamond (1992, 1994). Barton and Chou (1993) calculated the vapor-saturated liquidus surface in the H_2O-rich corner of the ternary. Few data are reported on the liquidi at higher NaCl and CO_2 concentrations (Chou, 1988; Schmidt et al., 1995).

A schematic phase diagram of the system H_2O-NaCl-CO_2 at elevated P-T conditions is shown in Figure 1. The diagram includes all of the various PVTX elements for which data were collected in this study. The ternary shows topological similarities to the binary H_2O-CO_2 with respect to the general shape of the immiscibility region (c.f., Takenouchi and Kennedy, 1964; Tödheide and Franck, 1963). An important difference that has significant implications for understanding fluid behavior in many high temperature and pressure environments is the expansion of the immiscibility field towards higher pressures and temperatures. The bubble-point/dew-point curves define the limits of the two-phase liquid-vapor region (immiscibility field) (L+V; Figure 1). For some compositions in the ternary, the solvus displays a local pressure minimum at moderate to high temperatures (P min; Figure 1). At temperatures below the temperature of the pressure minimum (towards high fluid densities), the solvus (bubble-point curve) pressure becomes increasingly less dependent on temperature for most compositions (Gehrig, 1980). At temperatures above the temperature of the pressure minimum, the solvus (dew-point curve) pressure increases gradually and reaches a maximum value. After passing through a pressure and temperature maximum, the dew-point curve shifts back towards lower temperatures and pressures (Figure 1). Although there are no experimental data, by analogy with the H_2O-NaCl binary system, a vapor + halite field should exist at low pressures (below the L+V field) for very dilute sodium chloride solutions due to the reduced NaCl solubility in vapor.

For compositions containing greater than about 25-30 wt% NaCl (relative to H_2O), the liquid and liquid + vapor fields are truncated at low temperatures by the halite liquidus (L+H; Figure 1). At pressures above the bubble-point curve, the liquidus separates the high temperature single-phase field (L; Figure 1) from the lower temperature region in which an NaCl-saturated liquid coexists with halite (L+H; Figure 1). At pressures below the bubble-point pressure, the liquidus separates a liquid+vapor field at higher temperature from a three-phase field at lower temperature in which liquid+vapor+halite coexist (L+V+H; Figure 1). The intersection of the liquidus with the bubble-point curve (P int; Figure 1) is equivalent to the intersection of the halite liquidus with the liquid-vapor curve in the H_2O-NaCl binary (c.f., Bodnar, 1994).

The slopes ($\Delta P/\Delta T$)of the isochores(or iso-Th lines) in the H_2O-NaCl-CO_2 system are steep for lower homogenization temperatures (higher densities), and become less steep as Th increases or density decreases. Thus, the slope of the isochore labeled “1” (Figure 1), representing an H_2O-NaCl-CO_2 inclusion that homogenizes to the liquid phase, is steeper than that of an inclusion with the same composition that has a lower density and homogenizes to the vapor phase (isochore “4”; Figure 1). The P-T path followed by an inclusion that homogenizes by critical behavior, as described in more detail below, must intersect the solvus at the critical point, and extrapolation of this isochore (isochore “2”; Figure 1) into the the one-phase region serves to divide fluids with liquid-like properties at pressures above the isochore, from fluids with vapor-like properties at pressures below the critical isochore. The pressure minimum on the solvus, described above, offers some unusual possibilities for isochoric P-T paths. Diamond (1996) suggested that some isochores in the H_2O-NaCl-CO_2 system may intersect the

solvus more than once (Figure 1, isochore "3"). Although this behavior has not been proven yet experimentally for this ternary system, Frantz et al. (1992) show some calculated isochores, based on synthetic fluid inclusion experiments, that intersect the solvus more than once. If this does occur for some PTX trapping conditions in the H_2O-NaCl-CO_2 ternary, it has important implications for the interpretation of results from natural samples.

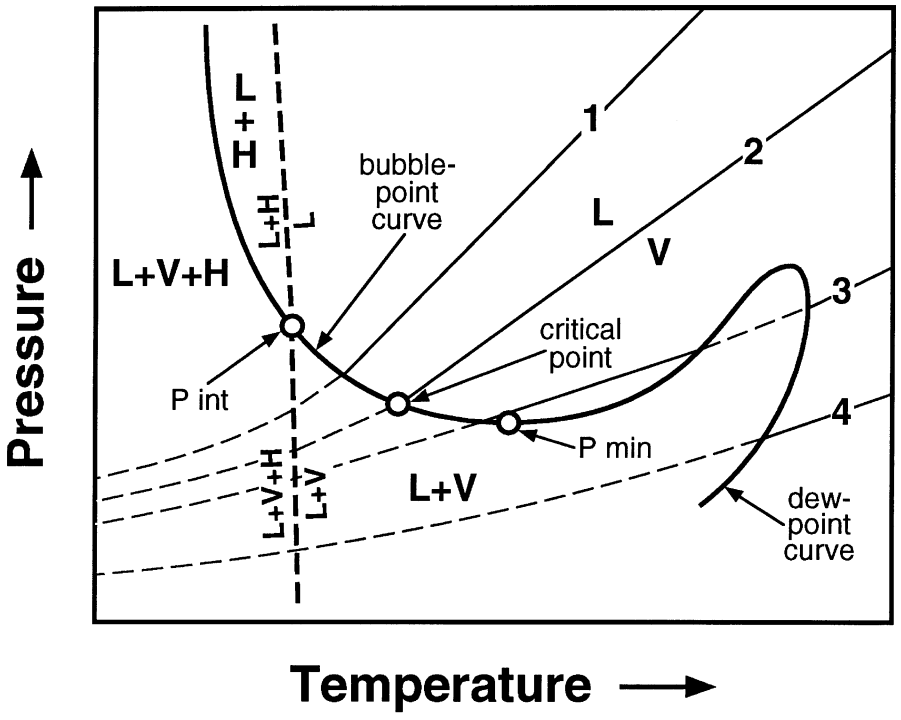

Figure 1. Schematic topology of the system water-sodium chloride-carbon dioxide at high P and T and applicable to compositions in the range of about 30 to 40 wt% NaCl and approximately 1 to 5 mol% CO_2. Heavy lines indicate boundaries of phase stability fields: solvus (heavy solid line), liquidus (heavy dashed line). L = liquid; V = vapor; L+V = coexisting liquid and vapor; L+H = coexisting liquid and halite; L+V+H = coexisting liquid, vapor, and halite. A liquid + halite field (L+H) should be present at relatively high NaCl concentrations and low mol fractions of carbon dioxide. The liquid-vapor curve (solvus) consists of the bubble-point curve (bulk density of the fluid greater than the critical density) and the dew-point curve (bulk density of the fluid less than the critical density). P min = local pressure minimum of the solvus; P int = point of intersection of liquidus (separating the L+H field from the L field, or separating the L+V+H field from the L+V field) with the liquid-vapor curve. Four different isochores are depicted as thin lines. Within the one-phase field these lines are solid; within the two- or three-phase fields these lines are dashed. High-density inclusions follow isochore 1 and homogenize to the water-rich, liquid phase; low-density mixtures homogenize to the CO_2-rich, vapor phase along isochore 4. Inclusions displaying critical homogenization behavior (at the critical point) follow the critical isochore (isochore 2) which divides the one-phase field into a liquid and a vapor field. Isochores of type 3 that intersect the liquid + vapor field twice may exist in this ternary system as suggested by Diamond (1996).

The interpretation of natural fluid inclusions depends largely on the availability of volumetric and phase equilibrium data. For the system H_2O-NaCl-CO_2, such data have been reported only over a limited range of temperatures, pressures, and NaCl concentrations. In this study, we used the synthetic fluid inclusion technique to extend the experimental conditions to 800°C, 6 kbar, and 40 wt% NaCl relative to water, and to determine solvus positions, lines of constant homogenization temperature (iso-Th lines), and critical properties, along with estimates of liquidus locations and molar volumes.

EXPERIMENTAL TECHNIQUES

Fluid inclusion synthesis. - All data reported in this study were obtained from synthetic fluid inclusions in quartz. During the last 15 years, the synthetic fluid inclusion technique has been established as a proven method for the determination of phase equilibria and volumetric properties in aqueous fluid systems containing salt and volatiles. The method is particularly advantageous in the study of high-salinity fluids at elevated temperature and pressure, because it avoids corrosion and fluid sampling problems associated with many conventional techniques. Details, uses and limitations of the synthetic fluid inclusion technique were described by Bodnar and Sterner (1987), Sterner and Bodnar (1984 and 1991) and Sterner (1992); the reader may refer to these papers for specific aspects outside the focus of this study. The experimental PTX conditions combined with microthermometric measurements of phase transitions in the inclusions yield information about phase equilibria and isochores at high P-T conditions.

Bulk compositions along three pseudobinaries in the system water-sodium chloride-carbon dioxide were studied:

(1) (H_2O + 6 wt% NaCl) - CO_2, having carbon dioxide concent-rations of 10 or 20 mol% relative to water,
(2) (H_2O + 20 wt% NaCl) - CO_2, including carbon dioxide concent-rations of 10, 20, 30, 50, or 70 mol% CO_2 relative to water, and
(3) (H_2O + 40 wt% NaCl) - CO_2, having carbon dioxide concent-rations of 5, 10, or 20 mol% carbon dioxide.

Starting materials to produce these compositions and a prefractured quartz core were loaded into platinum capsules, which were then sealed with an arc welder. If the desired fluid composition contained 6 or 20 wt% NaCl, silver oxalate ($Ag_2C_2O_4$) (used as the carbon dioxide source) was loaded first, followed by either a 6 or 20 wt% sodium chloride standard solution. The amount of solution added was calculated to give the desired H_2O/CO_2 ratio after silver oxalate decomposition. For 40 wt% NaCl compositions, thoroughly dried halite (NaCl) was added to the capsule first, followed by silver oxalate, and then deionized, distilled water until the salinity relative to water was within 40±0.1 wt% sodium chloride. Silica gel was not used in these experiments to avoid possible absorption of water from atmospheric moisture (Schmidt et al., 1995). The actual carbon dioxide yield of the silver oxalate was determined previously by decomposing a known amount of $Ag_2C_2O_4$ in sealed platinum capsules and measuring the weight loss after piercing the capsules (Sterner and Bodnar, 1991).

The sealed capsules and filler rods (to reduce thermal gradients) were loaded into cold-seal pressure vessels and run at the pressure and temperature of interest (2 to 5 kbar and 300°C to 700°C). An internally-heated pressure vessel (IHPV) was used for experimental conditions

of 800°C or 6 kbar. To minimize damage to the capsules due to silver oxalate decomposition, the vessels were pressurized to 500-700 bar at the start of the experiments. This pressure was maintained until the silver oxalate in the capsules decomposed at a temperature of about 200 to 250°C (Sterner and Bodnar, 1991). During heating to the final experimental temperature, the pressure in the vessels was gradually increased and (at temperatures above 300 to 400°C) occasionally cycled over a range of several hundred to a few thousand bars to minimize premature fracture healing and compositional heterogeneity of the fluid in the capsules (Bodnar and Sterner, 1987). The maximum pressure during cycling was mostly between 1 and 2.5 kbar higher than the expected solvus pressure to avoid entering the two-phase field. Once the experimental temperature was reached, the pressure was cycled several times between the experimental pressure and 1000-2000 bar above this pressure. Run durations varied according to the experimental temperature due to the dependence of quartz solubility (and thus fracture healing rates) on this variable: about 8 weeks for a formation temperature (Tf) of 300°C, approximately 4 weeks at Tf=400°C, 2 weeks at Tf=500°C, 4 to 6 days for Tf between 600°C and 700°C, and 1 to 3 days if Tf was 800°C. During that time, synthetic inclusions formed by entrapment of fluid in healed fractures or, at temperatures ≥500°C, by precipitating quartz as an overgrowth on the core. After completion of the experiments, the pressure vessels were cooled approximately isochorically.

After run completion, the capsules were dried, wrapped in tissue, equilibrated with the atmospheric moisture, weighed and then punctured. The weight loss within the first few seconds after puncturing, which is predominantly caused by loss of CO_2, was used to confirm if the actual carbon dioxide amount in the capsules corresponded to the CO_2 amount expected from the amount of silver oxalate. Although this technique is quite inaccurate if applied for samples which contain CO_2 and water (Sterner and Bodnar, 1991), the deviation was generally within 2% of the expected carbon dioxide amount. The quartz cores were then removed from the capsules, cut into small disks, polished on both sides, and examined using mainly petrographic and microthermometric techniques. Additionally, some samples were analyzed using Raman spectroscopy and SEM-EDS.

Microthermometry. - For inclusions having compositions along the 6 wt% and 20 wt% NaCl pseudobinaries, four phase transition temperatures were determined (Figure 2):

(1) the triple point of CO_2, i.e. the melting temperature of solid carbon dioxide in the presence of CO_2 liquid and vapor [Tm(CO_2)],
(2) the dissociation temperature of CO_2 hydrate in equilibrium with aqueous brine, and liquid and vapor carbon dioxide [Tm(CLA)],
(3) the homogenization temperature of the carbonic liquid and vapor phases [Th(CO_2)], and
(4) the temperature of total homogenization of CO_2-rich vapor and aqueous liquid to a single homogeneous phase [Th(L-V)].

The CO_2 triple point temperature (-56.6°C) was used to check the purity of the carbon dioxide in the inclusions. Tm(CLA) data yielded information about the inclusion salinity. For salt-free compositions (0 wt% NaCl), the clathrate dissociation temperature is 10.0°C, and this temperature decreases as salt is added (Chen, 1972; Bozzo et al., 1975; Darling, 1991; Diamond, 1992). The density of the carbonic phase at low temperature was obtained from Th(CO_2) (Lowry and Erickson, 1927). Additionally, the consistency of clathrate melting temperatures and the consistency of homogenization temperatures of the carbonic phases (if it occurred to the liquid) were applied as criteria for the homogeneity of the fluid samples at the experimental PTX conditions. Lines of equal homogenization temperature and most solvi were calculated based on the measured total homogenization temperatures as described below. If the inclusions contained 40 wt% sodium chloride relative to water, the temperature of halite

dissolution in equilibrium with aqueous liquid and CO_2-rich vapor [Tm halite] was measured instead of the clathrate dissociation temperature and was used to estimate liquidus positions.

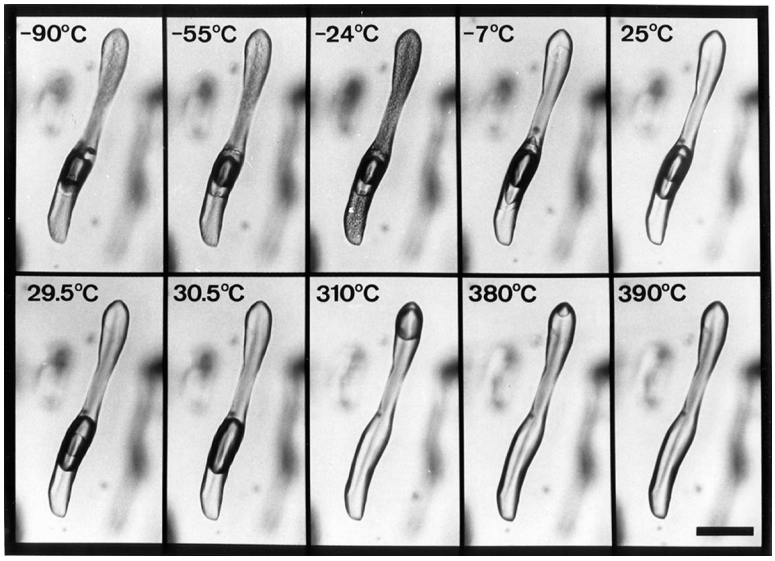

Figure 2. Heating and cooling behavior of a synthetic fluid inclusion containing H_2O + 20 wt% NaCl + 10 mol% CO_2. At -90°C, vapor, liquid CO_2, solid CO_2, CO_2 hydrate (clathrate), and hydrohalite coexist in the inclusion. The solid carbon dioxide phase melted at $Tm(CO_2)$ = -56.6°C. Solids in the inclusion recrystallized as evidenced by a darkening and coarsening of the crystals at temperatures of approximately -25 to -22°C. Hydrohalite started to dissociate rapidly at about -10°C. At -7°C, the inclusion contained a CO_2-rich vapor phase, liquid CO_2, aqueous brine, and clathrate (small isometric grain in aqueous liquid (top of inclusion) and solids adjacent to the liquid carbon dioxide phase). The dissociation temperature of the clathrate [Tm(CLA)] was -4.6°C. With further temperature increase, the CO_2-rich vapor phase became smaller and disappeared at $Th(CO_2)$ = 29.9°C. With further heating, the size of the vapor phase decreased and homogenization to the liquid [Th(L-V)] occurred at 388°C. The inclusion was synthesized at 650°C and 5 kbar. The scale bar equals 10 µm.

A Fluid Inc. adapted USGS-type gas-flow heating/freezing stage (Werre et al., 1979) was used for microthermometric measurements of phase transitions in the inclusions at one atmosphere external pressure. The thermocouple of this stage was routinely calibrated against the CO_2 triple point (-56.6°C), and the triple point (0.0°C) and critical point of water (374.1°C) using synthetic fluid inclusion standards (Sterner and Bodnar, 1984).

The smallest H_2O-NaCl-CO_2 inclusion that permits reliable determination of its homogenization temperature is about 10 μm. This size is somewhat larger than the usual minimum of about 2 to 3 μm, because the CO_2 bubble renucleates generally within a few °C of Th(L-V) upon cooling so that cycling techniques cannot be used. For a 10 μm inclusion, an internal pressure in excess of about 1.6 kbar can initiate stretching and decrepitation; larger inclusions require lower pressures (Bodnar et al., 1989). In this study, inclusions generating an internal pressure high enough to cause stretching and decrepitation during the heating runs were commonly encountered in samples having salinities ≥20 wt% NaCl and prevented determination of Th(L-V) if a gas-flow heating stage was used. Therefore, a hydrothermal diamond-anvil cell (HDAC) (Bassett et al., 1993; Chou et al., 1994) was used to exert a confining pressure on the sample during heating to obtain homogenization temperatures and halite dissolution temperatures of such inclusions.

The HDAC thermocouples were calibrated at the one-atmosphere melting points of azobenzene (68°C), sodium nitrate (306.8°C), and sodium chloride (801°C). The sample chamber of the hydrothermal diamond-anvil cell was loaded with the sample and water; water served as the confining pressure medium. Tm halite and Th(L-V) were measured for samples having bulk compositions of H_2O + 40 wt% NaCl + 10 mol% CO_2 and H_2O + 20 wt% NaCl + 20 mol% CO_2. The pressure in the chamber at the phase transition temperature was calculated from the density of the pressure medium (water) using the equation of Haar et al. (1984). The homogenization temperature of inclusions determined using the HDAC depends on the confining pressure (Schmidt et al., in preparation). Thus, Th(L-V) was measured for each sample at different (but known) confining pressures and normalized to a confining pressure equal to the estimated solvus pressure to correct for the effect of elastic volume change of the inclusion host quartz. The solvus pressure for these compositions was estimated from evidence of immiscibility in the run products by using petrographic and low-temperature microthermometric data. Details of the procedure used for the HDAC measurements are described by Schmidt et al. (in preparation).

To determine isochore slopes in the one-phase field for a particular composition, fluid inclusions were synthesized at different formation temperatures (Tf) along at least two formation pressure isobars (Pf) (Figure 3a). The total homogenization temperature Th(L-V) was measured for each sample and the formation temperatures were regressed as a function of Th(L-V) for each isobar (Figure 3b). Lines of constant homogenization temperature (iso-Th lines) were then obtained by solving the regression equations for each isobar for the same Th(L-V) value to determine (Tf, Pf) points on the iso-Th line corresponding to that homogenization temperature (Figure 3b and 3c). There is little difference between the slopes of iso-Th lines and the corresponding isochores. If the molar volume is known at any point along an iso-Th line, the iso-Th lines can be converted to isochores by correcting for the slightly nonisochoric behavior of the quartz host of the fluid inclusions, e.g. using the equation of state for α- and β-quartz of Hosieni et al. (1985) as described by Bodnar and Sterner (1985) and Sterner and Bodnar (1991). Linear fits to these P-T points were assumed to be sufficient to determine the dP/dT slopes of the isochores, because deviations of isochores from linearity in the one-phase field are normally small over the range of pressures and temperatures of this study and within the error associated with microthermometric measurements; furthermore, a slightly higher accuracy would only be achieved by a large increase in the number of required experiments.

Two different techniques were applied to obtain solvus pressures: (1) the "slope-intercept" technique (Sterner and Bodnar, 1991) and (2) delineation of the liquid + vapor field in P-T space using petrographic and microthermometric evidence (Bodnar et al., 1985). To calculate the pressure of the liquid-vapor curve using the "slope-intercept" approach, individual iso-Th lines were extrapolated to their corresponding total homogenization temperatures (Figure 3c). This method has the advantantage that the fluid composition is known accurately because the fluid inclusions are trapped in the single-phase field and thus theircomposition is identical to the known composition loaded into the capsule. The "slope-intercept" technique has been applied successfully to determine critical points and liquid-vapor curves in the systems H_2O-NaCl (Knight and Bodnar, 1989; Bodnar and Vityk, 1994), H_2O-CO_2 (Sterner and Bodnar, 1991), and H_2O-NaCl-CO_2 (Schmidt et al., 1995). However, the error in calculated solvus pressure associated with this method can be very large if iso-Th line slopes are steep and intersect a portion of the liquid-vapor curve that is almost independent of temperature. (Similarly, a large temperature error can result if the iso-Th lines are shallow and intersect a portion of the solvus that is almost pressure independent.) Therefore, an additional approach was used in conjunction with the "slope-intercept" technique to locate the immiscibility field. This technique brackets the formation pressures and temperatures of the experiments along isotherms or isobars. Samples which trapped a single phase, homogeneous fluid are characterized by fluid inclusions displaying consistent phase relations and consistent total homogenization temperatures which are less than their formation temperature, and constant salinities and densities of the CO_2-rich phase. Samples that show a large scatter in phase ratios, salinity, density of the CO_2-rich phase, and Th(L-V) data, and record total homogenization temperatures greater than or equal to the formation temperature of the sample indicate the presence of an unmixed fluid at the formation conditions (cp. Bodnar et al., 1985).

The critical isochore for a specific composition is obtained using a technique similar to the previously described procedures. Fluid inclusions having a bulk density higher than the critical density homogenize by shrinking of the vapor bubble and disappearance of the vapor phase at the homogenization temperature, and fluid inclusions of bulk densities lower than the critical density homogenize by expansion of the CO_2-rich vapor phase. If fluid inclusions of critical specific volume (density) are heated, the vapor density increases and the aqueous liquid density decreases towards the critical value; such fluids homogenize by fading and disappearance of the meniscus between liquid and vapor phases at the critical point. Along a given isobar, formation temperatures that bracket inclusions that homogenize by shrinking of the vapor bubble and those that homogenize by expansion of the vapor bubble were identified. Inclusions were then synthesized at increasingly smaller temperature steps within this range until inclusions homogenizing by critical behavior were obtained. The critical point pressure was then calculated by intersection of the critical isochore with the measured critical temperature, which can usually be determined with an accuracy of about ±5°C or better for temperatures below 500°C.

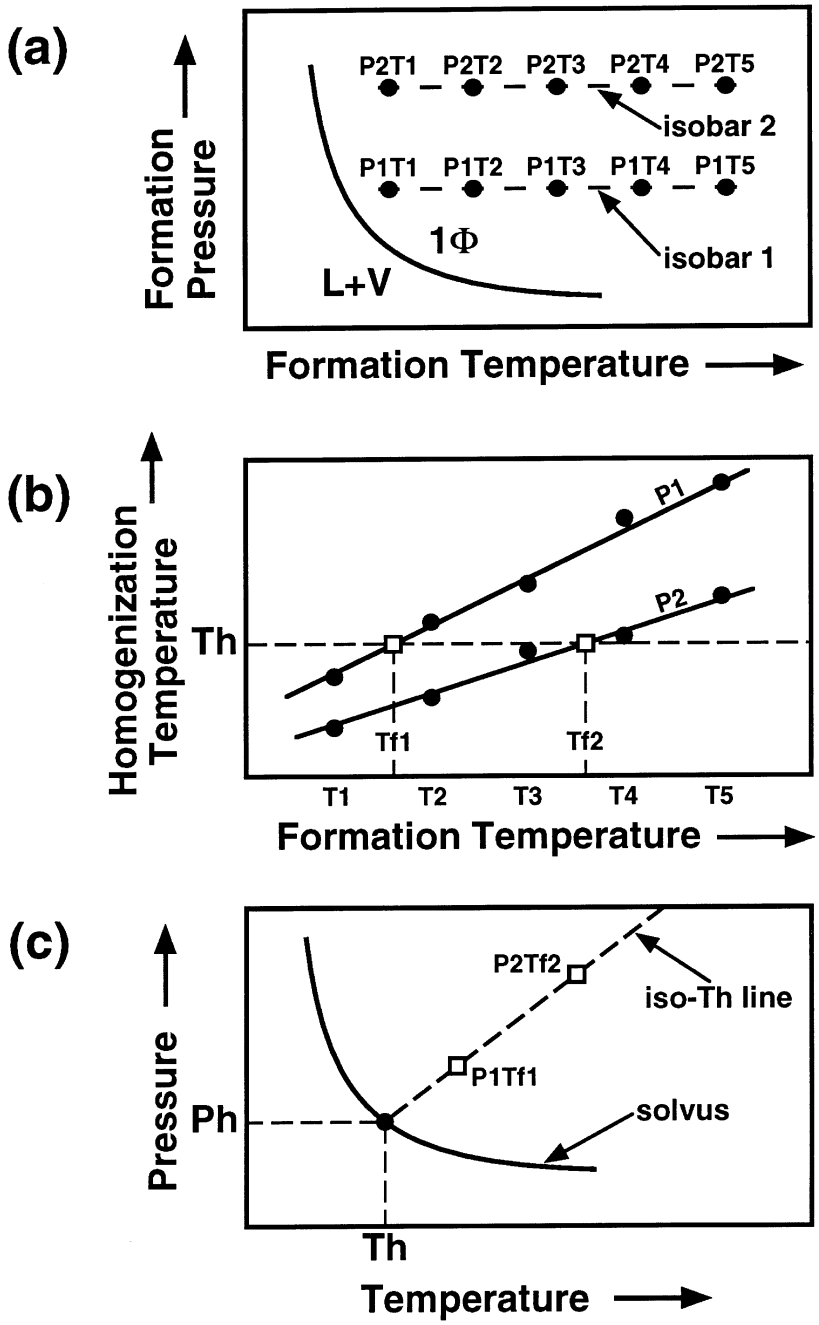

Figure 3. Schematic diagrams illustrating the procedure for determining iso-Th lines (a and b) and the "slope-intercept" technique to locate the liquid-vapor curve (c). T - temperature; P - formation pressure; Tf - formation temperature; Th - total homogenization temperature; Ph - homogenization pressure; L+V = liquid-vapor field; 1Φ - one-phase field.

Estimation of bulk molar volumes. - Bulk molar volumes of some samples were calculated following the procedure outlined by Schmidt et al. (1995). This calculation requires knowledge of the fluid bulk composition and the densities and compositions of the individual phases at some constant pressure and temperature. The density of the carbon dioxide-rich phase was determined at Th(CO_2) using microthermometry or at 32°C using Raman spectroscopy in conjunction with a temperature-controlled stage (Rosso and Bodnar, 1995). The composition of the carbonic phase was assumed to be pure carbon dioxide. For a H_2O + 87.5 mol% CO_2 mixture at Th(CO_2), this assumption results in a maximum error of about 1.5 % in the volume of the aqueous phase (Sterner and Bodnar, 1991). For ternary compositions studied here, the error is less than that, since the CO_2 concentrations were much lower (≤20 mol% CO_2 relative to water). Although the solubility of water in the carbonic phase of H_2O-NaCl-CO_2 solutions is not known, the assumption appears to be justified that the small amounts of water dissolved in the CO_2-rich phase at low temperature do not significantly affect the calculated density of that phase. The CO_2 pressure [P(CO_2)] corresponding to the measured density of the carbonic phase at Th(CO_2) or 32°C was obtained using either the equation of state for pure carbon dioxide of Duschek et al. (1990) at densities of less than or equal to 0.2 g/cm^3 or that of Bottinga and Richet (1981) if the density of the carbonic phase was above 0.2 g/cm^3. The solubility of CO_2 in the aqueous brine and the density of the aqueous solution at these temperatures and P(CO_2) was then calculated according to the equations given by Barton and Chou (1993). If the inclusions contained halite (in this study, this included all inclusions synthesized in the one-phase field along the (H_2O + 40 wt% NaCl) - CO_2 pseudobinary), the NaCl saturation concentration was estimated based on the equation of Sterner et al. (1988) for the binary H_2O-NaCl, and the density of the halite phase was taken as 2.163 g/cm^3 (Robie et al., 1979). The effect of carbon dioxide on the solubility of halite in aqueous brine was assumed to be negligible. The bulk molar volume of an inclusion in quartz at P(CO_2) and Th(CO_2) or at 32 °C was then converted to the molar volume at the formation temperature and the formation pressure by correcting for the volume change of quartz within this P-T interval as described above.

EXPERIMENTAL ERRORS

Compositional errors and solid phases in the inclusions. - Due to the presence of silica from the host mineral and silver from the decomposition of silver oxalate, the fluid system is more adequately described as H_2O-CO_2-NaCl-SiO_2-Ag. To our knowledge, no data are available for the solubility of quartz in H_2O-NaCl-CO_2 solutions at the temperatures and pressures of our experiments, which, however, is likely to be considerably smaller than the solubility of quartz in pure water. Based on the dissolution reaction

$$SiO_2(s) + 2H_2O = H_4SiO_4(aq), \quad (1)$$

the activity of silicic acid a(H_4SiO_4) is related to the square of the water activity $a^2(H_2O)$:

$$a(H_4SiO_4) = K \cdot a^2(H_2O), \quad (2)$$

where K is the equilibrium constant of reaction (1). The addition of NaCl or carbon dioxide, or both, will substantially lower the activity of water which results in $a^2(H_2O)$ significantly less than 1 and thus a decreased silica solubility. Evidence for this is also provided by the fact that the fluid in capsules loaded with quartz core and a ternary mixture run at high temperatures (600° to 800°C) and pressures (6 or 4 kbar) showed much less clouding from

colloidal silica formation when the capsule was opened after quenching than pure water + quartz samples run at the same conditions. The solubility of quartz in pure water is quite variable over most of the P-T range of fluid inclusion synthesis of this study: using the equation of Fournier and Potter (1982), it increases from 0.018 mol/kg H_2O (at 300°C and 2 kbar) to 0.53 mol/kg H_2O (which corresponds to about 3 wt% SiO_2 in solution) at 800°C and 4 kbar.

Bodnar and Sterner (1985) determined specific volumes of pure H_2O synthetic inclusions in quartz, which were formed at P-T conditions ranging from 1-3 kbar, 300-700°C, and corrected these for the thermal expansion of quartz using data from Skinner (1966). Most of these volumes agree within 1% with the data of Burnham et al. (1969). Sterner and Bodnar (1991) determined molar volumes of water up to 6 kbar and 700°C from synthetic fluid inclusions and corrected these based on the more recent equation of state of quartz by Hosieni et al. (1985); deviations from volumes reported by Burnham et al. (1969) and Haar et al. (1984) were about one percent or less. Schmidt et al. (in preparation) measured the compressibility of a pure H_2O synthetic inclusion in a hydrothermal diamond-anvil cell at different external pressures; the isochore corrected for the thermal expansion of quartz that corresponded to the homogenization temperature at 1 atmosphere external pressure (Th = 223°C) intersected the formation conditions of the inclusion (500 °C, 5 kbar) within ±5°C. Therefore, it can be assumed that the effect of silicic acid on the volumetric properties of water is small and affects solvus and isochore positions insignificantly.

Compared to silica, Ag or silver chloride may be a larger source of error. Silver is introduced into the system by the use of silver oxalate as the carbon dioxide source. An opaque phase occurs abundantly in healed fractures in the quartz as small isometric grains, blebs, rods, and occasionally tetrahedrons. This phase was identified as elemental silver using SEM-EDS and reflected light microscopy (native silver has an extremely high reflectivity). Opaque specks, isometric grains, rods, and tetrahedrons occur also in many fluid inclusions and are very likely native silver as well. The phase ratio of silver compared to fluid in the inclusions at room temperature can display a wide range in some fractures, where substantial amounts of excess silver were trapped accidentally. Inclusions in other healed fractures show uniform phase ratios of fluid and opaque phase, which in these cases has probably formed by precipitation of silver in solution during the run quench; this is also indicated by the observation that inclusions in fractures of samples formed at higher temperatures tend to possess slightly larger opaque phases than those having lower formation temperatures. Within the same sample, homogenization and halite dissolution temperatures of inclusions exhibiting relatively large silver crystals did not differ significantly from those of inclusions containing none or only a very small grain of native silver, suggesting that the silver is a trapped solid that was present in the fracture before the inclusions formed.

The enhanced silver solubility in chloride solutions at elevated P-T conditions had caused concerns about the applicability of silver oxalate in synthetic fluid inclusion studies (Plyasunova and Shmulovich, 1991). Data on the solubility of Ag in H_2O-NaCl-CO_2 fluids are not available; therefore, only a crude approximation can be given here. Experiments conducted by Seward (1976), Levin (1994) and Gammons and Williams-Jones (1995) up to 450°C and 1750 bar showed that the solubility of Ag in aqueous chloride solutions increases with temperature, oxygen fugacity, and Cl^- concentration and decreases with rising pH; pressure changes appear to have only a slight effect. Levin (1994) reported reduction of AgCl to metallic silver in pure water and in 0.92 mol NaCl/kg H_2O solution at 450°C and 1 kbar in a titanium autoclave. Silver solubility at 700°C, pH=5, Cl^- activity of 1 (molal) and an oxygen fugacity controlled by the pyrite + pyrrhotite + magnetite buffer assemblage is on the order of 1 to 10 wt% Ag; this estimate was obtained by extrapolating the solubility curve from Gammons and Williams-Jones (1995), which is based on the reaction

$$Ag(s) + 2Cl^- + H_2O = AgCl_2^- + OH^- + 0.5H_2(g). \quad (3)$$

However, equation (3) may be of little applicability to the experimental fluid system of this study, since the presence of carbon dioxide will lower the water activity and enhance the stability of metallic silver.

A strongly birefringent phase was detected in inclusions in some healed fractures in three samples that formed in the one-phase field (091295-VI, 042796-III, and 042796-VIII; 40 wt% NaCl, formation temperature 600°C or 700°C, run pressures 5 or 6 kbar). This phase occupied only a very small volume percent of the inclusions and was identified as nahcolite ($NaHCO_3$) using Raman spectroscopy. Nahcolite dissolution temperatures ranged from about 81° to 122°C. Inclusions from these samples which contained nahcolite displayed somewhat more irregular Th(L-V) and Tm(halite) and significantly lower CO_2 densities than inclusions where this phase was not detectable. The presence of nahcolite can be explained by the reaction:

$$H_2O + CO_2 + NaCl(aq) = NaHCO_3(aq) + HCl(aq). \quad (4)$$

Furthermore, at low pH and presence of metallic silver, the following reactions can produce $NaHCO_3$ and AgCl in solution:

$$2H_2O + 2CO_2 + 2NaCl(aq) + 2Ag = 2NaHCO_3(aq) + 2AgCl(aq) + H_2 \quad (5)$$

or, since $AgCl_2^-$ is the principal ionic species of silver in chloridic hydrothermal solutions around 300° to 400°C (Levin, 1994):

$$2H_2O + 2CO_2 + 2Na^+ + 2Cl^- + Ag = 2Na^+ + 2HCO_3^- + AgCl_2^- + 0.5H_2 + H^+. \quad (6)$$

Reaction (5) is probably a more representative description of speciation in the solution at temperatures of about 600° to 700°C, where ion pairs dominate. Both equations (5) and (6) indicate that AgCl formation requires a low hydrogen activity to counteract the decrease in water activity caused by addition of carbon dioxide and sodium chloride. In cold-seal vessels, the hydrogen fugacity is close to the Ni-NiO-H_2O buffer assemblage; at 700°C and 4 kbar, the fluid contains approximately 10 bars of H_2 due to dissociation of water (Sterner and Bodnar, 1991). The presence of hydrogen would favor metallic Ag as the more stable phase at most experimental conditions. The occasional occurrence of nahcolite at high fluid salinities and formation temperatures ≥600°C and pressures ≥5 kbar suggests that possibly significant amounts of sodium bicarbonate and AgCl are dissolved at these rather extreme conditions. The decrease of AgCl solubility with temperature implies the presence of solid silver chloride at room temperature. However, we have never observed solid AgCl in an inclusion, while euhedral native silver, halite, and nahcolite coexisted in some inclusions at ambient temperature. At room temperature, silver chloride might occur as thin coatings on the inclusion walls (Chou, personal communication). We did not detect any solid phases in the inclusions other than metallic silver and solids belonging to the system H_2O-CO_2-NaCl. No measurements from samples containing solid $NaHCO_3$ were used for the determination of iso-Th lines, solvi, and liquidi.

Iso-Th line slopes and solvus locations obtained in this study for a bulk composition of H_2O + 10 mol% CO_2 + 6 wt% NaCl in equilibrium with Ag are in relatively good agreement with data determined by Gehrig (1980) for practically the same composition in the absence of silver (Figure 4). Differences between the datasets are more likely due to pressure-temperature errors, e.g. the accurate determination of dP/dT isochore slopes is considerably more difficult

at lower solvus temperatures, where a large change in slope occurs over a small change in homogenization temperature. Furthermore, halite dissolution temperatures of H_2O + 10 mol% CO_2 + 40 wt% NaCl measured in this study are about 20 degrees higher than the vapor-saturated halite liquidus of an aqueous solution containing 40 wt% NaCl (Bodnar, 1994). Assuming that the shift in halite dissolution temperature is not related to the presence of carbon dioxide in the fluid and exclusively due to an effect of Ag or AgCl in solution, the maximum compositional error would be about 1.7 wt% NaCl relative to water using the equation of Sterner et al. (1988). Clathrate melting temperatures in the presence of aqueous brine, liquid CO_2, and CO_2-rich vapor for inclusions containing 6, 10, and 20 wt% NaCl (Table 3) are in very good agreement with the data of Diamond (1992) and the experimental results for the "pure" H_2O-NaCl-CO_2 system by Chen (1972). This indicates that the effect of AgCl on this univariant equilibrium is negligible and/or the AgCl concentration in solution is small. Because volatiles can have a great effect on solvus positions, accurate control of the CO_2 concentration was essential in this study. Thus, silver oxalate as carbon dioxide source was here considered as the better choice compared to the use of dry ice, which can result in relatively large errors in the water/carbon dioxide ratio, or oxalic acid, which results in experimental difficulties due to the presence of a large hydrogen concentration after its decomposition.

The uncertainty associated with weighing the individual masses of solids and liquids during the loading process is ≤0.0001 g, which corresponds to a 0.2% error for an average mass of 0.05 g per loaded substance. A somewhat larger, but known, compositional error can result from the difficulty of accurately adjusting the weights of solid NaCl and silver oxalate during capsule loading. The carbon dioxide yield of the silver oxalate batch used for all runs except 051396 was checked frequently by decomposing known amounts of $Ag_2C_2O_4$ in a sealed Pt capsule and determining the weight loss after piercing; it averaged between 99.6 and 99.3%. The uncertainty in CO_2 yield of silver oxalate as determined from weight loss measurements before loading of H_2O-NaCl-CO_2 capsules was approximately 0.5%. The CO_2 yield of the other batch was 98.4±0.2%. Lowering and scattering of the yield was prevented effectively by storage of the silver oxalate in vacuum and limiting the exposure to light and atmospheric moisture to a minimum.

Measurements of the melting temperature of solid carbon dioxide in equilibrium with vapor and liquid CO_2 [Tm(CO_2)] were used to determine the purity of the carbon dioxide in the synthesized inclusions. The Tm (CO_2) of most samples was within ±0.2°C (the uncertainty of the temperature measurements) of the triple point temperature of pure carbon dioxide (-56.6°C). Inclusions in some samples showed a slight depression of the CO_2 triple point down to -57.4°C indicating the presence of small amounts of another gas. In a few of these inclusions, traces of methane were identified using Raman spectroscopy. This occasional contamination should not have a significant effect on phase equilibria due to the low concentrations. Samples with lowered Tm(CO_2) and detectable methane had generally run durations of several weeks and formation temperatures of 400°C and 450°C.

The actual salinity of inclusions formed in the one-phase field and containing ≤20 wt% NaCl relative to water was repeatedly checked using dissociation temperatures of the CO_2 hydrate and generally deviated by at most ±1 wt% from the expected value (Appendix; Table 3). Therefore, water loss which can occur during capsule welding was insignificant. We estimate the overall uncertainty in the H_2O/NaCl and H_2O/CO_2 ratio to be within ±0.2 wt% NaCl and ±0.5 mol% CO_2 of the values of the individual runs listed in the appendix (Tables 1 to 4).

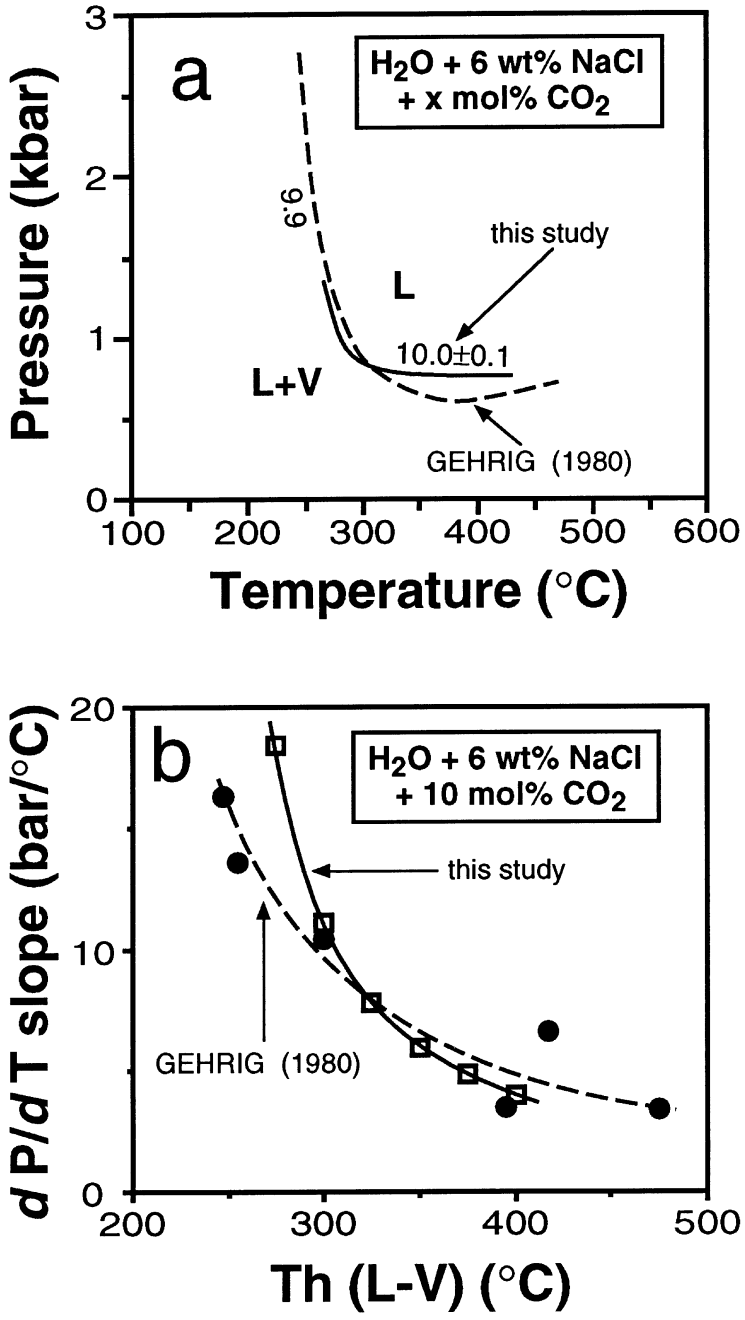

Figure 4. Comparison of the experimental data for a high-pressure part of the solvus (a) and isochore slopes (b) obtained by Gehrig (1980) and in this study for the bulk composition H_2O + 6 wt% NaCl + 10 mol% CO_2.

Pressure-temperature errors. - The uncertainty in experimental pressure and temperature of cold-seal pressure vessels used here is about ±1 % (Sterner and Bodnar, 1991). The pressure in the cold-seal bombs was measured using a Bourdon tube-type Heise gauge and a manganin cell. The calibration of both was checked against a factory calibrated transducer, which was also used to monitor the pressure in the IHPV. Up to 4.9 kbar, differences in pressure readings between these three devices were less than 30 bar. To evaluate the error in experimental temperature due to thermal gradients, platinum capsules (length 2.0 to 2.5 cm) containing pure water and a fractured quartz core were placed behind the H_2O-CO_2-NaCl capsules (that is, towards the "cold" end of the cold-seal pressure vessel) and run at the same pressures and set temperatures. (The average length of the H_2O-CO_2-NaCl capsules was about 3 cm). The homogenization temperatures of the pure H_2O synthetic inclusions formed during these runs were then used to calculate isochores based on the specific volumes of water given by Haar et al. (1984), which were corrected for thermal expansion of quartz using the equation of Hosieni et al. (1985). The formation temperature of the pure water inclusions was then calculated by intersecting these isochores with the corresponding experimental pressures. These calculated formation temperatures were within 10°C of the thermocouple temperatures. The uncertainty in experimental temperature in the IHPV is about ±10° at 800°C; the pressure error is approximately ±1%. The thermal gradient across the platinum capsule length of about 4 cm was estimated to be 5°C (J. Student, personal communication).

Microthermometric measurements in the gas-flow stage have the following estimated accuracies: ±0.5°C at about -50 to -60°C, approximately ±0.2°C between -10°C and +30°C, and better than ±2 degrees Celsius for temperature measurements up to 400°C. Above that temperature, the accuracy decreases to about ±5 degrees Celsius at 600°C. Temperatures determined using a hydrothermal diamond-anvil cell have a similar or perhaps somewhat lower uncertainty (cp. Shen et al., 1993). Homogenization temperatures of some samples show a slightly higher scatter than would be expected based on the uncertainty of the microthermometric measurements. These samples formed in the one-phase field as indicated by measured Th(L-V) that were less than the run temperature. The source of error due to relatively large scattering of Th(L-V) could not always be eliminated, although such runs were generally repeated using more frequent cycling of the bomb pressure above the expected solvus pressure before the samples equilibrated at the final experimental P and T, and can be explained by two effects: (1) Slight compositional heterogeneities in the fluid may occur if the P-T conditions of the run were close to the solvus, particularly in samples having high salinities and carbon dioxide concentrations. Furthermore, the solvus of such compositions is mostly located at high pressures and temperatures; therefore, those samples required a relatively long time to pass through the immiscibility field before the runs equilibrated at the pressures and temperatures of interest. (2) At temperatures above 600°C, the solubility of silica appears to be high enough that fractures in the quartz core may heal prematurely and trap inclusions before the final run temperature and pressure was attained.

RESULTS AND DISCUSSION

Liquid-vapor curves and iso-Th lines. - Iso-Th lines in the one-phase field and high pressure portions of the liquid-vapor curve were determined for six compositions:

H_2O + 40 wt% NaCl + 5 mol% CO_2,
H_2O + 40 wt% NaCl + 10 mol% CO_2,
H_2O + 20 wt% NaCl + 10 mol% CO_2,
H_2O + 20 wt% NaCl + 20 mol% CO_2,
H_2O + 6 wt% NaCl + 10 mol% CO_2, and
H_2O + 6 wt% NaCl + 20 mol% CO_2.

Figure 5 shows the corresponding phase diagrams in P-T space which can be applied to the study of natural fluid inclusions. The solvus for H_2O + 6 wt% NaCl + 20 mol% CO_2 was interpolated from the data published by Gehrig (1980) which was more accurate than calculations based on the Th(L-V) data of the few samples of this composition synthesized in this study. For the compositions H_2O + 40 wt% NaCl + 10 mol% CO_2 and H_2O + 20 wt% NaCl + 20 mol% CO_2, the liquid-vapor curve locations were obtained by delineation of the one-phase field based on petrographic and microthermometric evidence for the absence of unmixing. The iso-Th lines were calculated from Th(L-V) data normalized to the solvus pressure, since these homogenization temperatures were determined at different confining pressures using a hydrothermal diamond-anvil cell (Appendix; Table 1). All other iso-Th lines and solvi shown are based on homogenization temperatures measured at one atmosphere confining pressure using a gas-flow stage (Appendix; Table 1), and do not require corrections. Table 5 (Appendix) lists linear regression equations of formation temperature [Tf] as a function of homogenization temperature [Th] along isobars of formation pressure. All iso-Th line slopes derived from homogenization temperature data obtained in this study and those liquid-vapor curves that were located using the "slope-intercept" technique (i.e. the solvi of the compositions H_2O + 6 wt% NaCl + 10 mol% CO_2, H_2O + 20 wt% NaCl + 10 mol% CO_2, and H_2O + 40 wt% NaCl + 5 mol% CO_2) were calculated from these equations.

The slopes of iso-Th lines at a constant homogenization temperature increase along pseudobinaries with addition of carbon dioxide and particularly with addition of NaCl (Figure 6), which partly reflects collapse of the water structure. In the compositional range up to 20 mol% CO_2 and at constant salinity, the high-pressure portion of the solvus shifts to significantly higher pressures and temperatures as the carbon dioxide concentration increases. The same effect was observed for a constant H_2O/CO_2 ratio with addition of NaCl (Figure 7). In the pseudobinary (H_2O + 20 wt% NaCl) - CO_2, the solvus expands rapidly towards very high pressures and temperatures if the CO_2 concentration exceeds 20 mol%. Samples of the compositions H_2O + 20 wt% NaCl + 30 to 70 mol% CO_2 showed clear evidence of unmixing at all P-T conditions up to 700°C and 5 kbar, with the possible exception of the 30 mol% CO_2 run at 5 kbar formation pressure and 700°C formation temperature. This confirms the conclusion of Johnson (1991) that immiscibility is possible in this ternary system even at granulite-facies P-T conditions at salinities above 23 wt% NaCl and intermediate mol fractions of carbon dioxide ($XCO_2 > 0.3$).

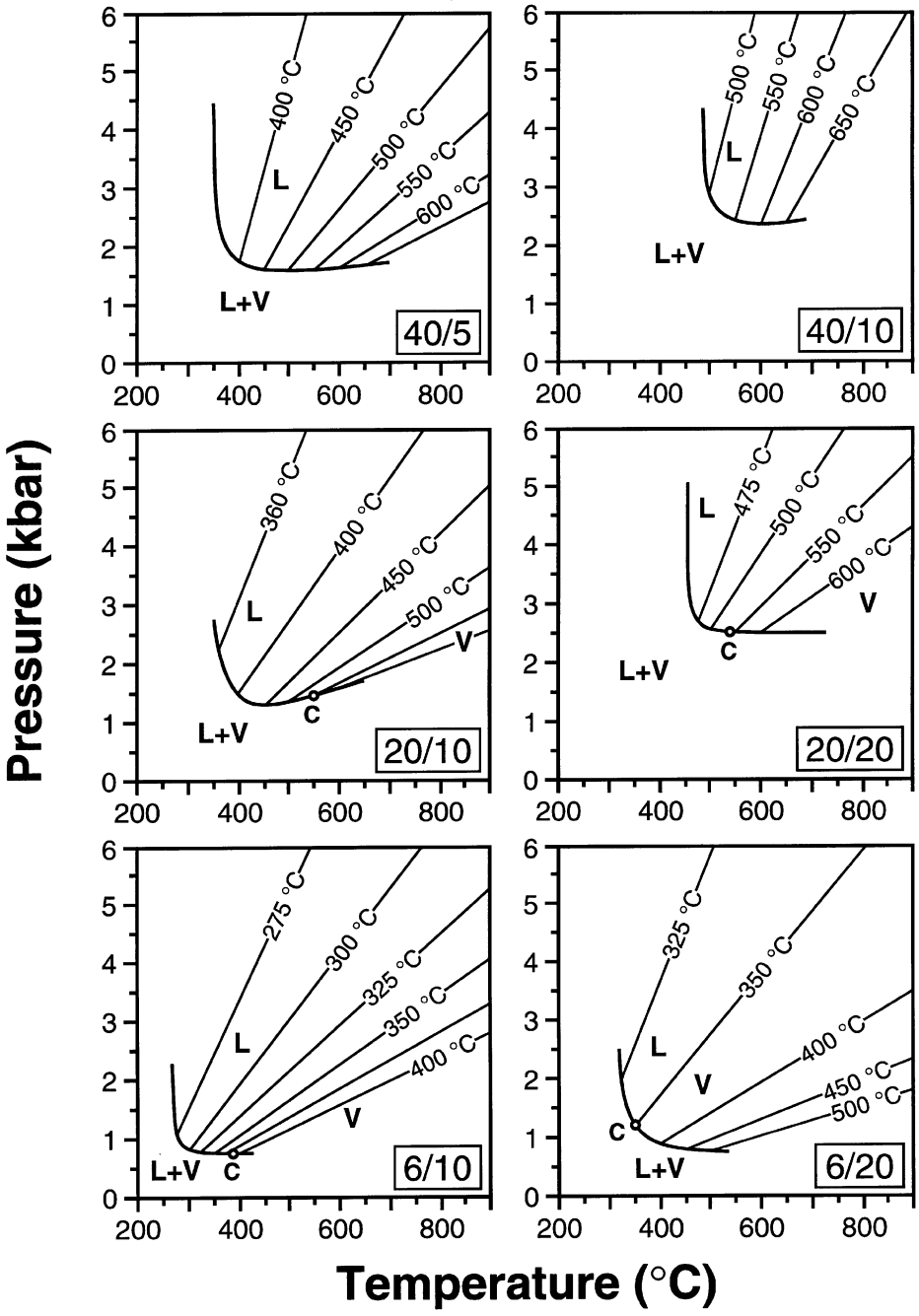

Figure 5. Iso-Th lines in the one-phase field and high pressure portions of the liquid-vapor curve as determined in this study for the following bulk compositions: 40/5 = H_2O + 40 wt% NaCl + 5 mol% CO_2; 40/10 = H_2O + 40 wt% NaCl + 10 mol% CO_2; 20/10 = H_2O + 20 wt% NaCl + 10 mol% CO_2; 20/20/ = H_2O + 20 wt% NaCl + 20 mol% CO_2; 6/10 = H_2O + 6 wt% NaCl + 10 mol% CO_2; 6/20 = H_2O + 6 wt% NaCl + 20 mol% CO_2. The solvus for H_2O + 6 wt% NaCl + 20 mol% CO_2 was interpolated from data published by Gehrig (1980). L = liquid; V = vapor; L+V = liquid + vapor; C = critical point.

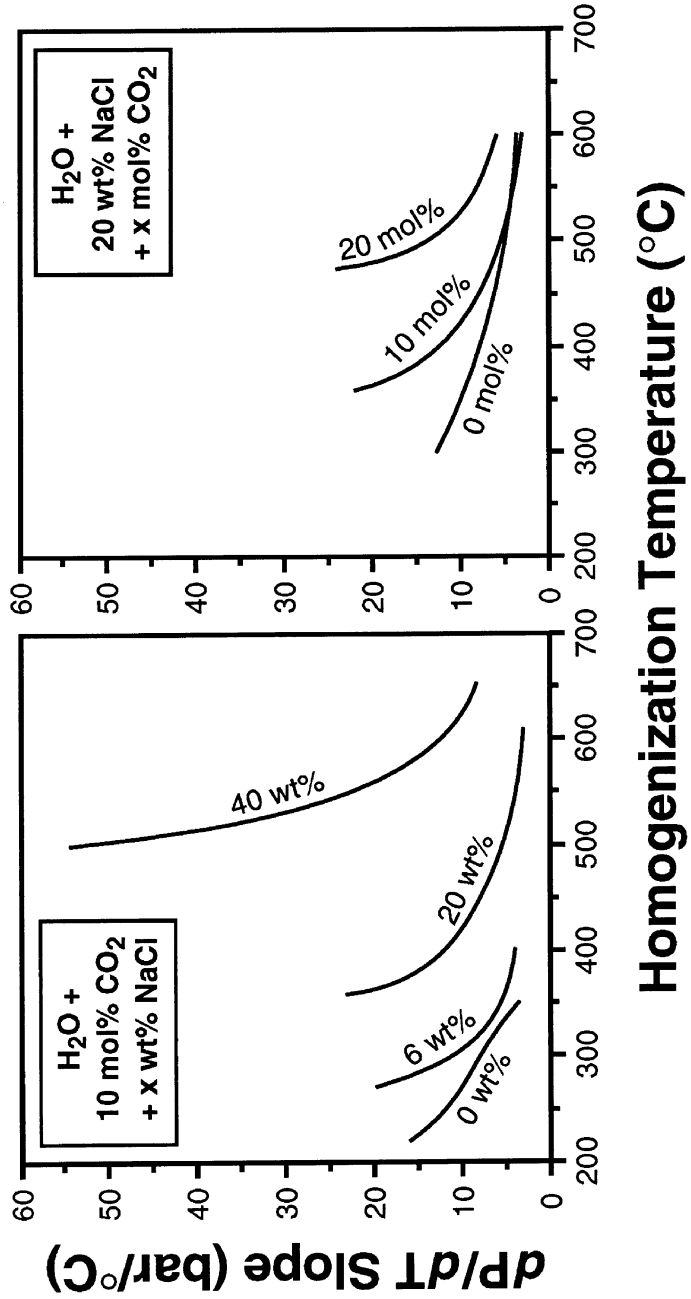

Figure 6. Isochore slopes as a function of homogenization temperature along two pseudobinaries in the system H_2O-NaCl-CO_2. Data for H_2O + 10 mol% CO_2 are from Connolly and Bodnar (1983), and slopes of H_2O + 20 wt% NaCl are from Bodnar and Vityk (1994). Slopes of ternary mixtures were calculated from homogenization temperatures obtained in this study.

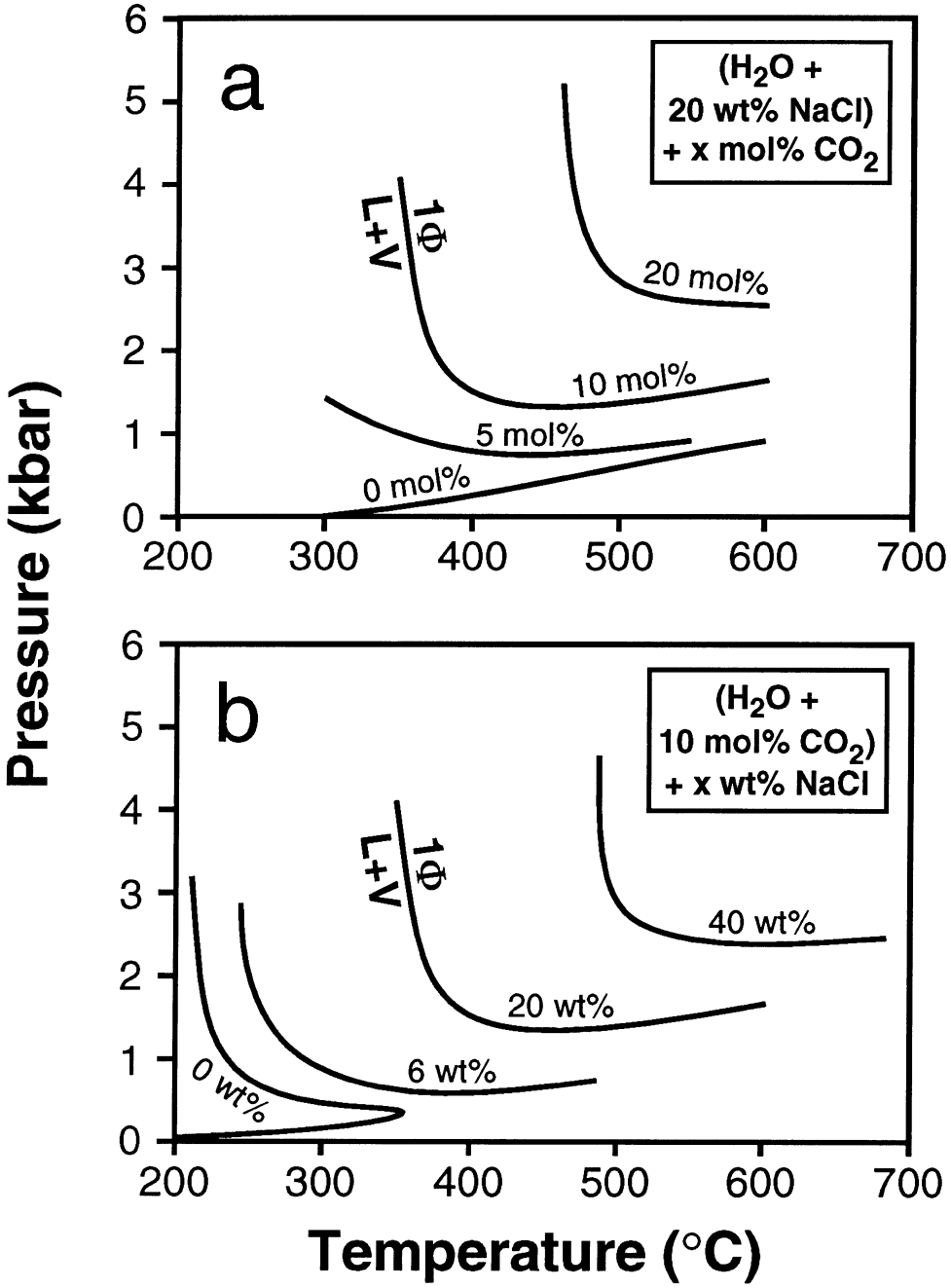

Figure 7. High-pressure portions of liquid-vapor curves of the pseudobinaries (H_2O + 20 wt% NaCl) - CO_2 (a) and (H_2O + 10 mol% CO_2) - NaCl (b). The solvus of H_2O + 10 mol% CO_2 is from Takenouchi and Kennedy (1964), he liquid-vapor curve for H_2O + 20 wt% NaCl was obtained from Bodnar and Vityk (1994), and the solvi for H_2O + 6 wt% NaCl + 10 mol% CO_2 and H_2O + 20 wt% NaCl + 5 mol% CO_2 are from Gehrig (1980).

Critical properties. - Physical and thermodynamic properties of aqueous solutions, such as heat capacity and viscosity, show extrema in the critical region in P-T space (Pitzer, 1986). Knowledge of critical properties in the system H_2O-NaCl-CO_2 is, therefore, of importance for numerical simulations of crustal fluid-flow and fluid-rock interaction (Bodnar and Costain, 1991) and supercritical water oxidation technology (Bodnar, 1995). In this study, critical temperatures and pressures were determined for bulk compositions up to 20 wt% NaCl and 20 mol% CO_2, both relative to water. The obtained critical surface is plotted along pseudobinaries in Figure 8. Addition of carbon dioxide in this compositional range results in a rapid increase of the critical pressure and slightly lower critical temperatures, whereas the main consequence of a rise in NaCl concentration is the sharp increase in critical temperature. Thus, the net effect of addition of both sodium chloride and carbon dioxide is generally a shift of the critical point towards much higher pressure and temperature.

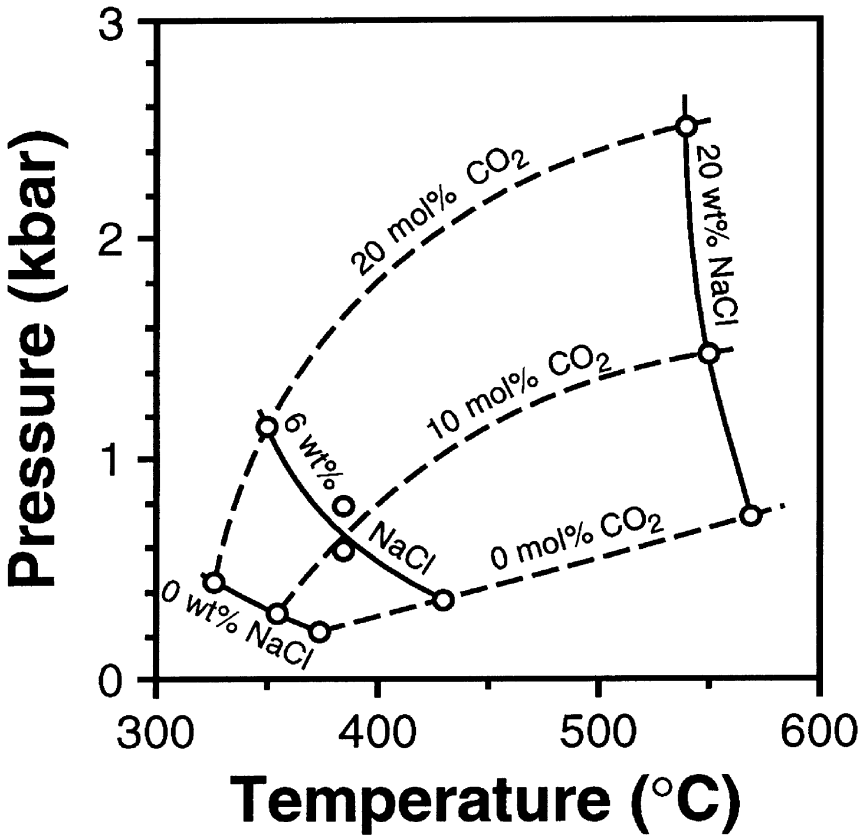

Figure 8. P-T plot of the upper critical surface in the system water-sodium chloride-carbon dioxide along constant H_2O/NaCl ratios up to 20 wt% NaCl and H_2O/CO_2 ratios to 20 mol% CO_2. Data for the binary H_2O-CO_2 are from Tödheide and Franck (1963) and for H_2O-NaCl from Knight and Bodnar (1989). The critical points for ternary mixtures are based on the experimental determinations of this study.

Halite liquidi. - Halite dissolution temperatures in equilibrium with aqueous brine and CO_2-rich vapor [Tm halite] were determined for 40 wt% NaCl samples (Appendix; Table 2). All measured inclusions in this pseudobinary had consistently higher halite dissolution temperatures than the vapor-saturated halite liquidus temperature of 323°C for a 40 wt% NaCl solution obtained by Bodnar (1994). A slight positive correlation between Tm halite and Th(L-V) was found for inclusions containing 5 mol% CO_2 relative to water. The bubble-point curve may intersect the halite liquidus for this composition at a very high pressure outside the experimental pressure range of this study. If that point of intersection exists, it occurs at about 329°C. This was calculated by linear regression of the total homogenization and halite dissolution temperature data and extrapolating that line to Tm halite = Th(L-V). No relationship between Tm halite and Th(L-V) was found for a bulk carbon dioxide concentration of 10 mol%. At this composition, the temperature of the equilibrium halite + liquid + vapor = liquid + vapor averaged 342±6°C and appeared to be practically independent of pressure up to about 2 kbar (decrepitation occurred rarely at that temperature). There was generally very good agreement between halite dissolution temperatures determined using a gas-flow heating stage and those measured in a diamond-anvil cell at high confining pressure (Schmidt et al., in preparation). A further elevation of Tm halite was observed for samples having a bulk composition of H_2O + 40 wt% NaCl + 20 mol% CO_2. The increase of halite dissolution temperature with carbon dioxide concentration could be caused by the presence of carbon dioxide in the aqueous phase and/or can be a result of water loss from the aqueous liquid phase to the carbonic vapor phase. The latter interpretation is supported by comparison to the system NaCl-H_2O, where a similar correlation exists between the dissolution temperature of halite in vapor-saturated liquid and the corresponding liquid-vapor homogenization temperature (Chou, 1987). The elevated Tm halite may also be in part due to dissolved AgCl in the aqueous brine.

Densities of the CO_2-rich phase and molar volume calculations. - For most samples, Th(CO_2) was measured mainly as a check to confirm that inclusions were trapped in the one-phase field (Appendix; Table 4). Molar volumes were calculated for some samples based on densities of the CO_2-rich phase using the procedure outlined in Schmidt et al. (1995). At bulk compositions of H_2O + 6 wt% NaCl + 10 or 20 mol% CO_2, pressures of 2 or 3 kbar, and temperatures of 400°C, 450°C, and 500°C, direct comparison to the molar volume data reported by Gehrig (1980) is possible. Figure 9 shows the difference between the data obtained by Gehrig (1980) and the calculated molar volumes of this study plotted as a function of the density of the carbon dioxide-rich phase, which, in turn, depends on the bulk molar volume. Most of the calculated volumes are about 2 cm^3/mol higher than the corresponding experimental data of Gehrig (1980). This is a substantial difference, since the absolute values for the molar volume at these PTX conditions are relatively small and range only between about 24 and 32 cm^3/mol (Gehrig et al., 1986). The deviation can be much larger close to the carbon dioxide critical density, where microthermometric measurements of the carbon dioxide density are insensitive due to the very small change in Th(CO_2) over a significant density variation in this region. If CO_2 homogenization is to the vapor phase (at CO_2 densities less than about 0.47 g/cm^3), it is very difficult to observe the evaporation of the last liquid CO_2 optically, and the corresponding carbon dioxide density can only be considered as a minimum value (Sterner and Bodnar, 1991). Surprisingly, the molar volume deviation is approximately the same regardless of whether the CO_2 density was higher or lower than the critical carbon dioxide density. A potential alternative is the determination of the density of the CO_2-rich phase using Raman spectroscopy in conjunction with a temperature-controlled Joule-Thompson optical stage (Rosso and Bodnar, 1995; Schmidt et al., 1995), but this technique may not have the resolution yet to increase the accuracy significantly. Good spectra are so far only obtained for inclusions having a large CO_2 bubble. Even at CO_2 densities above about 0.5 g/cm^3, carbon dioxide densities obtained using Raman spectroscopy and microthermometry can differ substantially; an example is deviation of about 0.1 g/cm^3 in the data for sample 031295-7 (20 wt% NaCl, 20 mol% CO_2; see Appendix, Table 4), which contained very large inclusions

displaying a very small range in Th(CO_2) to the liquid and was considered to be very suitable for the application of both techniques.

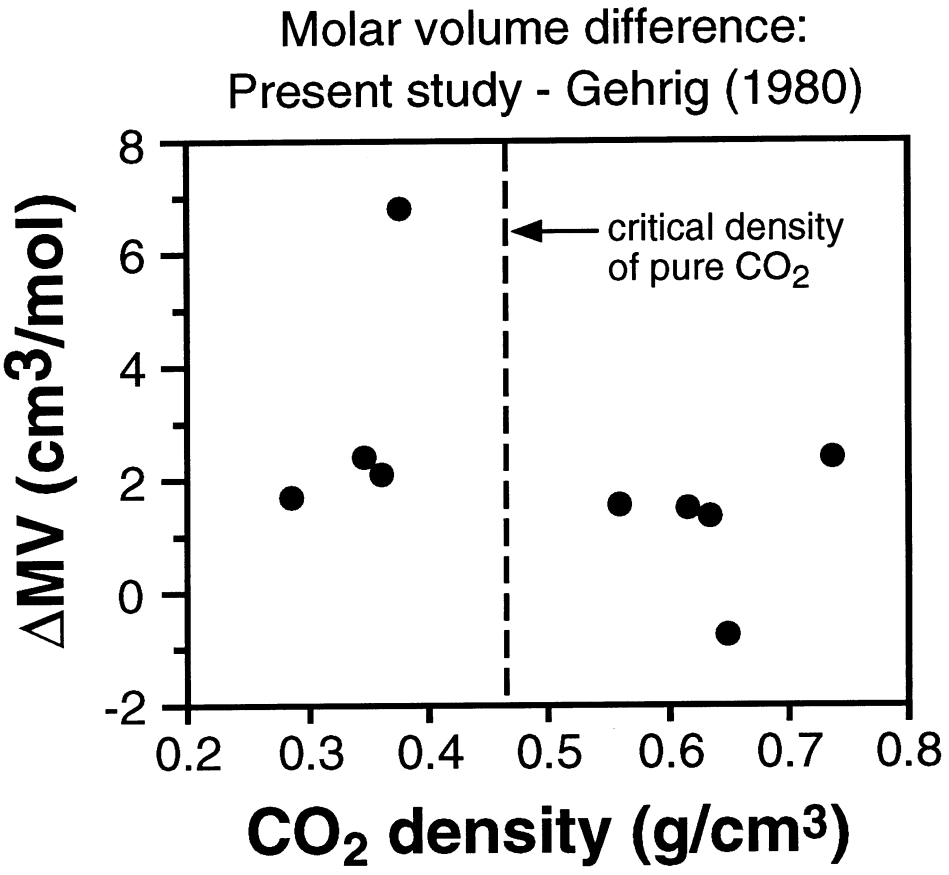

Figure 9. Plot of bulk molar volumes of ternary H_2O-NaCl-CO_2 mixtures calculated from the partial homogenization temperature of the CO_2-rich phases [Th(CO_2)] obtained in this study minus the experimentally determined molar volume by Gehrig (1980) at the same PTX conditions vs. the microthermometrically obtained density of the carbonic phase at Th(CO_2). Also shown is the critical density of pure carbon dioxide (approximately 0.468 g/cm^3).

SUMMARY

Using the synthetic fluid inclusion technique, dP/dT slopes of iso-Th lines, high-pressure portions of solvi, critical properties, and halite dissolution temperatures in equilibrium with vapor and aqueous liquid were determined for water-rich compositions in the ternary system H_2O-NaCl-CO_2. The previously available database was extended to salinities of 40 wt% NaCl, compositions up to 20 mol% CO_2 relative to water, temperatures to 800°C, and pressures up to 6 kbar. The dataset for homogenization temperatures was converted to isoplethic phase diagrams in P-T space. The experimental results reported here are highly relevant for the interpretation of natural fluid inclusions and supercritical water oxidation technology for the treatment of hazardous organic waste.

Addition of NaCl or carbon dioxide, or both, to water has a profound effect on solvus and critical point location. The obtained data show that immiscibility can occur over a very wide range of PTX conditions and is possible even in deeper crustal rocks. The critical point shifts rapidly to higher pressures and temperatures with rising NaCl and CO_2 concentration. The dP/dT slopes of lines of equal homogenization temperature increase with salinity and carbon dioxide concentration and decrease with homogenization temperature. Both isochore slopes and solvus positions within the (H_2O + 6 wt% NaCl) - CO_2 pseudobinary are in good agreement with the experimental determination of Gehrig (1980). Halite dissolution temperatures in presence of liquid and vapor show a slight dependence on the relative carbon dioxide amount of the bulk composition.

REFERENCES

Anderko A. and Pitzer K. S. (1993) Equation of state representation of phase equilibria and volumetric properties of the system NaCl-H_2O above 573 K. *Geochim. Cosmochim. Acta* **57**, 1657-1680.

Barton P. B. and Chou I-M. (1993) Calculation of the vapor-saturated liquidus for the NaCl-CO_2-H_2O system. *Geochim. Cosmochim. Acta* **57**, 2715-2723.

Bassett W. A., Shen A. H., Bucknum M., and Chou I-M. (1993) A new diamond anvil cell for hydrothermal studies to 2.5 GPa and from -190 to 1200 °C. *Rev. Sci. Instrum.* **64**, 2340-2345.

Blencoe J. G., Seitz J. C., Anovitz L. M., Joyce D. B., and Bodnar R. J. (1996) Thermodynamic mixing properties of C-O-H-N fluids at high pressures and temperatures. In *Reactivity and Mobility of Geologic Fluids: Constraints from Inorganic Geochemistry. Symp. ORNL Prog. Abstr.*, 10.

Bodnar R. J. (1994) Synthetic fluid inclusions: XII. Experimental determination of the halite liquidus and isochores for a 40 wt.% H_2O-NaCl solution. *Geochim. Cosmochim. Acta* **58**, 1053-1063.

Bodnar, R. J. (1995) Applications of synthetic fluid inclusions in supercritical water oxidation research. *Proc. 12th International Conference on the Properties of Water and Steam*, Beggel House, Inc., 644-651.

Bodnar R. J. and Sterner S. M. (1985) Synthetic fluid inclusions in natural quartz. II. Application to PVT studies. *Geochim. Cosmochim. Acta* **49**, 1855-1859.

Bodnar R. J. and Sterner S. M. (1987) Synthetic fluid inclusions. In *Hydrothermal Experimental Techniques* (ed. G. C. Ulmer and H. L. Barnes), pp. 423-457. Wiley.

Bodnar, R. J. and Costain, J. K. (1991) Effect of fluid composition on mass and energy transport in the earth's crust. *Geophys. Res. Letters* **18**, 983-986.

Bodnar R. J. and Vityk M. O. (1994) Interpretation of microthermometric data for H_2O-NaCl fluid inclusions. In *Fluid Inclusions in Minerals, Methods and Applications* (ed. B. De Vivo and M. L. Frezotti), pp. 117-130. Virginia Tech, Blacksburg, VA.

Bodnar R. J., Burnham C. W., and Sterner S. M. (1985) Synthetic fluid inclusions in natural quartz. III. Determination of phase equilibrium properties in the system H_2O-NaCl to 1000 °C and 1500 bars.*Geochim. Cosmochim. Acta* **49**, 1861-1873.

Bodnar R. J., Binns P. R., and Hall D. L. (1989) Synthetic fluid inclusions. VI. Quantitative evaluation of the decrepitation behavior of fluid inclusions in quartz at one atmosphere confining pressure. *J. Metam. Geol.* **7**, 229-242.

Bottinga Y. and Richet P. (1981) High pressure and temperature equation of state and calculation of the thermodynamic properties of gaseous carbon dioxide. *Amer. J. Sci.* **281**, 615-660.

Bowers T. S. and Helgeson H. C. (1983a) Calculation of the thermodynamic and geochemical consequences of nonideal mixing in the system H_2O-CO_2-NaCl on phase relations in geologic systems: Equation of state for H_2O-CO_2-NaCl fluids at high pressures and temperatures. *Geochim. Cosmochim. Acta* **47**, 1247-1275.

Bowers T. S. and Helgeson H. C. (1983b) Calculation of the thermodynamic and geochemical consequences of nonideal mixing in the system H_2O-CO_2-NaCl on phase relations in geologic systems: Metamorphic equilibria at high pressures and temperatures. *Amer. Mineral.* **68**, 1059-1075.

Bozzo A. T., Chen H-S., Kass J. R., and Barduhn A. J. (1975) The properties of the hydrates of chlorine and carbon dioxide. *Desalination* **16**, 303-320.

Brown P. E. and Lamb W. M. (1989) P-V-T properties of fluids in the system $H_2O \pm CO_2 \pm$ NaCl: New graphical presentations and implications for fluid inclusion studies. *Geochim. Cosmochim. Acta* **53**, 1209-1221.

Burnham C. W., Holloway J. R., and Davis N. F. (1969) Thermodynamic properties of water to 1000 °C and 10,000 bars. *Geol. Soc. Amer. Spec. Paper No. 132*.

Chen H-S. (1972) The thermodynamics and composition of carbon dioxide hydrate. M.Sc. thesis, Syracuse Univ.

Chou I-M. (1987) Phase relations in the system NaCl-KCl-H_2O. III. Solubilities of halite in vapor-saturated liquids above 445 °C and redetermination of phase equilibrium properties in the system NaCl-H_2O to 1000 °C and 1500 bars. *Geochim. Cosmochim. Acta* **51**, 1965-1975.

Chou I-M. (1988) Halite solubilities in supercritical carbon dioxide-water fluids. *GSA Abstr. Prog.* **20**, A76.

Chou I-M., Shen A. H., and Bassett W. A. (1994) Applications of the hydrothermal diamond-anvil cell in fluid inclusion research. In *Fluid Inclusions in Minerals, Methods and Applications* (ed. B. De Vivo and M. L. Frezotti), pp. 215-230. Virginia Tech, Blacksburg, VA.

Connolly J. A. D. and Bodnar R. J. (1983) A modified Redlich-Kwong equation of state for H_2O-CO_2 mixtures - Application to fluid inclusion studies. *EOS, Transactions* **64**, 350.

Darling, R. S. (1991) An extended equation to calculate NaCl contents from final clathrate melting temperatures in H_2O-CO_2-NaCl fluid inclusions: Implications for P-T isochore location. *Geochim. Cosmochim. Acta* **55**, 3869-3871.

Diamond, L. W. (1992) Stability of CO_2 clathrate hydrate + CO_2 liquid + CO_2 + aqueous KCl-NaCl solutions: Experimental determination and application to salinity estimates of fluid inclusions. *Geochim. Cosmochim. Acta* **56**, 273-280.

Diamond, L. W. (1994) Salinity of multivolatile fluid inclusions determined from clathrate hydrate stability.*Geochim. Cosmochim. Acta* **58**, 19-41.

Diamond, L. W. (1996) Isochoric paths in immiscible fluids and the interpretation of multicomponent fluid inclusions. *PACROFI VI Prog. Abstr.*, 36-37.

Drummond S. E., Jr. (1981) Boiling and mixing of hydrothermal fluids: Chemical effects on mineral precipitation. Unpubl. Ph.D. Dissertation, Penn. State Univ.

Duan Zh., Møller N., and Weare J. H. (1995) Equation of state for the NaCl-H_2O-CO_2 system: Prediction of phase equilibria and volumetric properties. *Geochim. Cosmochim. Acta* **59**, 2869-2882.

Duschek W., Kleinrahm R., and Wagner W. (1990) Measurement and correlation of the (pressure, density, temperature) relation of carbon dioxide. I. The homogeneous gas and liquid regions in the temperature range from 217 K to 340 K at pressures up to 9 MPa. *J. Chem. Thermodyn.* **22**, 827-840.

Ellis A. J. and Golding R. M. (1963) The solubility of carbon dioxide above 100 °C in water and in sodium chloride solutions. *Amer. J. Sci.* **261**, 47-60

Fournier R. O. and Potter R. W. II (1982) An equation correlating the solubility of quartz in water from 25 ° to 900 °C at pressures up to 10,000 bars. *Geochim. Cosmochim. Acta* **46**, 1969-1973

Frantz J. D., Popp R. K., and Hoering T. C. (1992) The compositional limits of fluid immiscibility in the system H_2O-NaCl-CO_2 as determined with the use of synthetic fluid inclusions in conjunction with mass spectrometry. *Chem. Geol.* **98**, 237-255.

Gammons C. H. and Williams-Jones A. E. (1995) The solubility of Au-Ag alloy + AgCl in HCl/NaCl solutions at 300 °C: New data on the stability of Au(I) chloride complexes in hydrothermal fluids.*Geochim. Cosmochim. Acta* **59**, 3453-3468.

Gehrig M. (1980) Phasengleichgewichte und pVT-Daten ternärer Mischungen aus Wasser, Kohlendioxid und Natriumchlorid bis 3 kbar und 550 °C. Doctoral dissertation, Univ. Karlsruhe.

Gehrig M., Lentz H., and Franck E. U. (1986) The system water-carbon dioxide-sodium chloride to 773 K and 300 MPa. *Ber. Bunsenges. Phys. Chemie* **90**, 525-533.

Haar L., Gallagher J. S., and Kell G. S. (1984) NBS/NRC Steam Tables: Thermodynamic and Transport Properties and Computer Programs for Vapor and Liquid States of Water in SI Units. Hemisphere Publ. Co.

Hosieni K. R., Howald R. A., and Scanlon M. W. (1985) Thermodynamics of the lambda transition and the equation of state of quartz. *Amer. Mineral.* **70**, 782-793

Johnson E. L. (1991) Experimentally determined limits for H_2O-CO_2-NaCl immiscibility in granulites. *Geology* **19**, 925-928.

Johnson E. L. (1992) An assessment of the accuracy of isochore location techniques for H_2O-CO_2-NaCl fluids at granulite facies pressure-temperature conditions. *Geochim. Cosmochim. Acta* **56**, 295-302.

Joyce D. B. and Holloway J. R. (1993) An experimental determination of the thermodynamic properties of H_2O-CO_2-NaCl fluids at high pressures and temperatures.*Geochim. Cosmochim. Acta* **57**, 733-746.

Knight C. L. and Bodnar R. J. (1989) Synthetic fluid inclusions: IX. Critical PVTX properties of NaCl-H_2O solutions.*Geochim. Cosmochim. Acta* **53**, 3-8.

Kotelnikov A. R. and Kotelnikova Z. A. (1990) An experimental study of the phase state of the system H_2O-CO_2-NaCl using synthetic fluid inclusions in quartz. *Geokhimiya* **4**, 526-537 (in Russian).

Labotka T. C. (1991) Chemical and physical properties of fluids. In *Rev. Mineral.* **26**, 43-104.

Levin, K. A. (1994) Thermodynamic properties of silver chloride complexes. *Geochem. Intl.* **31** (7), 41-47.

Lowry, H. H. and Erickson W. R. (1927) The densities of coexisting liquid and gaseous carbon dioxide and the solubility of water in liquid carbon dioxide. *J. Amer. Chem. Soc*. **49**, 2729-2734

Malinin S. D. and Savelyeva N. I. (1972) The solubility of CO_2 in NaCl and $CaCl_2$ solutions at 25, 50, and 75 ° under elevated CO_2 pressures. *Geochem. Intl.* **9**, 410-417.

Malinin S. D. and Kurovskaya N. A. (1975) Solubility of CO_2 in chloride solutions at elevated temperatures and CO_2 pressures. *Geochem. Intl.* **12**, 199-201.

Pitzer K. S. (1986) Large-scale fluctuations and the critical behavior of dilute NaCl in H_2O. *J. Phys. Chem*. **90**, 1502-1504.

Plyasunova N. V. and Shmulovich K. I. (1991) Phase equilibria in the system H_2O-CO_2-$CaCl_2$ at 500 °C. *Transactions (Doklady) USSR Acad. Sci.* **320**, 7, 221-225.

Robie R. A., Hemingway B. S., and Fisher J. R. (1979) Thermodynamic properties of minerals and related substances at 298.15 K and 1 bar (10^5 Pascals) pressure and at higher temperatures. *USGS Bull*. **1452**.

Roedder E. (1984) Fluid Inclusions. *Rev. Mineral.* **12**.

Rosso K. M. and Bodnar R. J. (1995) Microthermometric and Raman spectroscopic detection limits of CO_2 in fluid inclusions and the Raman spectroscopic characterization of CO_2. *Geochim. Cosmochim. Acta* **59**, 3961-3975.

Schmidt C., Rosso K. M., and Bodnar R. J. (1995) Synthetic fluid inclusions: XIII. Experimental determination of PVT properties in the system H_2O + 40 wt% NaCl + 5 mol% CO_2 at elevated temperature and pressure.*Geochim. Cosmochim. Acta* **59**, 3953-3959.

Schmidt C., Chou I-M., Bodnar R. J., and Bassett, W. A. (in preparation) Microthermometric analyses of synthetic fluid inclusions using the hydrothermal diamond-anvil cell.

Seward T. M. (1976) The stability of chloride complexes of silver in hydrothermal solutions up to 350 °C.*Geochim. Cosmochim. Acta* **40**, 1329-1341.

Shaw, R. W., Brill, T. B., Clifford, A. A., Eckert, C. A. and Franck, E. U. (1991) Supercritical water: a medium for chemistry. Chem. & Eng. News **69**, no.51, 26-39.

Shen A. H., Bassett W. A., and Chou I-M. (1993) The α-β quartz transition at high temperatures and pressures in a diamond-anvil cell by laser interferometry. *American Mineralogist* **78**, 694-698

Shmulovich K. I. and Plyasunova N. V. (1993) Phase equilibria in ternary systems formed by H_2O and CO_2 with $CaCl_2$ or NaCl at high P and T. *Geochem. Intl.* **30**, 53-71.

Skinner, B. J. (1966) Thermal expansion. In *Handbook of Physical Constants,* Revised Edn. (ed. S. P. Clark) *Geol. Soc. Amer. Mem. 97,* 75-96.

Sourirajan S. and Kennedy G. C. (1962) The system H_2O-NaCl at elevated temperatures and pressures. *Amer. J. Sci.* **260**, 115-141.

Sterner S. M. (1992) Synthetic fluid inclusions. XI. Notes on the application of synthetic fluid inclusions to high P-T experimental aqueous geochemistry. *Amer. Mineral.* **77**, 156-167.

Sterner S. M. and Bodnar R. J. (1984) Synthetic fluid inclusions in natural quartz. I: Compositional types synthesized and applications in experimental geochemistry. *Geochim. Cosmochim. Acta* **48**, 2659-2668.

Sterner S. M. and Bodnar R. J. (1991) Synthetic fluid inclusions. X: Experimental determination of *P-V-T-X* properties in the CO_2-H_2O system to 6 kb and 700 °C. *Amer. J. Sci.* **291**, 1-54.

Sterner S. M., Hall D. L., and Bodnar R. J. (1988) Synthetic fluid inclusions. V. Solubility relations in the system NaCl-KCl-H_2O under vapor-saturated conditions. *Geochim. Cosmochim. Acta* **52**, 989-1005

Takenouchi S. and Kennedy G. C. (1964) The binary system H_2O-CO_2 at high temperatures and pressures. *Amer. J. Sci.* **262**, 1055-1074.

Takenouchi S. and Kennedy G. C. (1965) The solubility of carbon dioxide in NaCl solutions at high temperatures and pressures. *Amer. J. Sci.* **263**, 445-454.

Tester, J. W., Holgate, H. R., Armellini, F. J., Webley, P. A., Killilea, W. R., Hong, G. T., Barner, H. E. (1992) Supercritical water oxidation technology: a review of process development and fundamental research. *1991 ACS Symposium Series: Emerging Technologies for Hazardous Waste Management III,* Atlanta, GA.

Tödheide K. and Franck E. U. (1963) Das Zweiphasengebiet und die kritische Kurve im System Kohlendioxid-Wasser bis zu Drucken von 3500 bar. *Zeitschr. Phys. Chemie Neue Folge* **37**, 387-401.

Werre R. W., Jr., Bodnar R. J., Bethke P. M., and Barton P. B., Jr. (1979) A novel gas-flow fluid inclusion heating/freezing stage (abstr.). *Geol. Soc. Amer. Abstr.with Prog.* **11**, 539.

Yasunishi A. and Yoshida F. (1979) Solubility of carbon dioxide in aqueous electrolyte solutions. *J. Chem. Eng. Data* **24**, 11-14.

APPENDIX

Table 1. Liquid-vapor homogenization temperatures and experimental conditions for synthetic fluid inclusions in the H_2O-NaCl-CO_2 system

Tf = formation temperature (°C); Pf = formation pressure (kbar); Salinity = NaCl concentration of the solution in weight percent relative to H_2O; Mol% CO_2 = carbon dioxide concentration in mol percent relative to H_2O; Th(L-V) (average) = average liquid-vapor homogenization temperature (°C); Th(L-V) (range) = the range in measured Th(L-V) (°C); (L) = homogenization to the liquid, aqueous phase); (V) = homogenization to the vapor, CO_2-rich phase); (C) = homogenization by critical behavior; n = number of measured inclusions; GHFS = gas-flow heating/freezing stage; HDAC = hydrothermal diamond-anvil cell; n.d. = not determined

Sample Number	Tf	Pf	Salinity	Mol% CO_2	Th(L-V) (average)	Th(L-V) (range)	n	Method
012196-3	400	2.0	6	10	295 (L)	290 - 300	33	GHFS
012196-4	500	2.0	6	10	333 (L)	330 - 338	32	GHFS
012196-8	600	2.0	6	10	363 (L)	358 - 367	41	GHFS
031196-9	650	2.0	6	10	379 (L)	374 - 383	35	GHFS
031196-10	675	2.0	6	10	385 (C)	381 - 389	43	GHFS
021896-4	700	2.0	6	10	395 (V)	392 - 398	25	GHFS
012196-1	400	3.0	6	10	280 (L)	274 - 284	43	GHFS
012196-2	500	3.0	6	10	303 (L)	297 - 311	32	GHFS
012196-9	600	3.0	6	10	327 (L)	323 - 330	25	GHFS
021896-8	700	3.0	6	10	350 (L)	346 - 353	42	GHFS
050396-5	800	3.0	6	10	372 (L)	365 - 379	52	GHFS
021896-3	400	4.0	6	10	272 (L)	263 - 277	36	GHFS
021896-7	500	4.0	6	10	284 (L)	280 - 289	38	GHFS
031196-3	600	4.0	6	10	301 (L)	297 - 306	31	GHFS
021896-1	700	4.0	6	10	321 (L) 334 (L)	317 - 325 328 - 340	33 5	GHFS GHFS
031196-4	700	4.0	6	10	317 (L)	311 - 319	34	GHFS
012196-5	400	2.0	6	20	329 (L)	315 - 334	33	GHFS
012196-6	450	2.0	6	20	327 (L)	323 - 337	21	GHFS
012196-7	500	2.0	6	20	356 (V)	354 - 361	14	GHFS
040496-1	550	2.0	6	20	381 (V)	374 - 388	19	GHFS
021896-5	600	2.0	6	20	408 (V)	401 - 416	23	GHFS
040496-2	650	2.0	6	20	452 (V)	440 - 467	21	GHFS
031196-1	700	2.0	6	20	498 (V)	486 - 509	8	GHFS
021896-9	400	3.0	6	20	319 (L)	315 - 322	25	GHFS
021896-10	500	3.0	6	19.8	327 (L)	322 - 335	32	GHFS
021896-11	500	3.0	6	20	330 (L)	326 - 336	32	GHFS
031196-5	600	3.0	6	20	347 (L) 350 (C) 351 (V)	344 - 354 346 - 355 346 - 357	26 8 7	GHFS GHFS GHFS
040496-3	700	3.0	6	20	370 (V)	367 - 377	25	GHFS
050396-4	800	3.0	6	20	417 (V)	408 - 425	25	GHFS
112594-2	450	3.5	10	10	302.5 (L)	301 - 304	20	GHFS

Table 1 (continued)

Sample Number	Tf	Pf	Salinity	Mol% CO_2	Th(L-V) (average)	Th(L-V) (range)	n	Method
011895-9	300	2.0	20	9.9	immiscible fluid			
011895-3	350	2.0	20	10	immiscible fluid?			
011895-4	400	2.0	20	10	376 (L)	374 - 378	9	GHFS
031295-5	450	2.0	20	10	400 (L)	391 - 407	24	GHFS
011895-6	500	2.0	20	10	415 (L)	411 - 418	13	GHFS
041395-11	550	2.0	20	10	458 (L)	450 - 466	44	GHFS
011895-1	600	2.0	20	10	494 (L)	487 - 497	16	GHFS
020295-4	650	2.0	20	10	533 (L)	525 - 543	32	GHFS
011895-2	700	2.0	20	10	594 (V,C)	588 - 600	5	GHFS
041395-10	400	3.0	20	10	362 (L)	356 - 365	17	GHFS
042395-9	450	3.0	20	10	379 (L)	374 - 383	21	GHFS
042395-7	500	3.0	20	10	394 (L)	390 - 398	23	GHFS
062895-4	500	3.0	20	10	393 (L)	386 - 397	34	GHFS
042395-1	550	3.0	20	10	408 (L)	401 - 412	39	GHFS
041395-6	600	3.0	20	10	433 (L)	426 - 436	27	GHFS
062895-3	600	3.0	20	10	433 (L)	428 - 444	36	GHFS
042395-3	650	3.0	20	10	453 (L)	446 - 460	20	GHFS
062895-2	650	3.0	20	10	444 (L)	431 - 459	39	GHFS
062895-1	700	3.0	20	9.9	467 (L)	457 - 480	35	GHFS
050396-3	800	3.0	20	9.9	498 (L,C) 538 (L,C)	495 - 501 536 - 540	13 9	GHFS GHFS
011895-7	300	4.0	20	10	immiscible fluid			
031295-1	400	4.0	20	10	353 (L)	346 - 358	13	GHFS
031295-4	450	4.0	20	10	363 (L)	360 - 366	22	GHFS
011895-8	500	4.0	20	10	378 (L)	376 - 381	15	GHFS
041395-7	550	4.0	20	10	385 (L)	383 - 388	40	GHFS
031295-2	600	4.0	20	10	405 (L)	402 - 414	36	GHFS
031295-3	650	4.0	20	10	418 (L)	413 - 421	42	GHFS
020295-5	700	4.0	20	10	427 (L)	418 -432	24	GHFS
040496-5	800	4.0	20	9.9	433 (L)	430 - 436	36	GHFS
042395-8	450	5.0	20	10	356 (L)	353 -357	8	GHFS
042395-5	500	5.0	20	10	360 (L)	358 - 362	34	GHFS
042395-4	550	5.0	20	9.9	368 (L)	365 - 373	33	GHFS
042395-6	600	5.0	20	10	378 (L)	374 - 382	25	GHFS
062895-5	650	5.0	20	10	388 (L)	382 - 402	53	GHFS
062895-6	700	5.0	20	10	402 (L)	394 - 411	30	GHFS
020295-8	400	2.0	20	20	immiscible fluid			
022695-1	450	2.0	20	20.1	immiscible fluid			
020295-7	500	2.0	20	20.1	immiscible fluid			
022695-4	600	2.0	20	20	immiscible fluid			
022695-3	650	2.0	20	19.9	immiscible fluid			
022695-2	700	2.0	20	20.1	immiscible fluid			

Table 1 (continued)

Sample Number	Tf	Pf	Salinity	Mol% CO_2	Th(L-V) (average)	Th(L-V) (range)	n	Method
032595-3	400	3.0	20	20	immiscible fluid			
051595-4	450	3.0	20	20	immiscible fluid			
051595-3	500	3.0	20	20	473 (L) 479 (L)	466 - 481 477 - 481	10 2	GHFS HDAC
071195-4	550	3.0	20	19.9	516 (L)	514 - 518	9	GHFS
032595-2	600	3.0	20	20	577 (V) 545 (C,V)	574 - 582 539 - 551	4 3	GHFS HDAC
060695-6	650	3.0	20	20	591 (V)	589 - 595	5	GHFS
032595-4	700	3.0	20	20	631 (V) 608 (V)	622 - 639 598 - 618	13 2	GHFS HDAC
060695-2	400	4.0	20	20	immiscible fluid			
060695-1	450	4.0	20	20	immiscible fluid			
060695-3	500	4.0	20	20	462 (L)	460 - 464	3	HDAC
111195-5	550	4.0	20	20	n.d.			
031295-7	600	4.0	20	20	n.d.			
060695-4	650	4.0	20	20	n.d.			
031295-6	700	4.0	20	20	556? (V) 540 (C,L)	 530 - 550	1 2	GHFS HDAC
071195-1	400	5.0	20	20	immiscible fluid			
071195-2	450	5.0	20	19.9	immiscible fluid			
060695-5	500	5.0	20	20	455 (L)	452 - 458	2	HDAC
071195-3	550	5.0	20	20	n.d.			
051595-2	600	5.0	20	20.1	480 (L)	476 - 484	6	HDAC
062895-7	700	5.0	20	20	n.d.			
062895-8	500	3.0	20	29.9	immiscible fluid			
080895-3	400	4.0	20	29.9	immiscible fluid			
102495-4	500	4.0	20	30	immiscible fluid			
071195-5	600	4.0	20	29.9	immiscible fluid			
080895-8	700	4.0	20	30	immiscible fluid			
080895-2	400	5.0	20	29.9	immiscible fluid			
102495-2	450	5.0	20	29.9	immiscible fluid			
080895-5	500	5.0	20	30	immiscible fluid			
102495-1	550	5.0	20	30	immiscible fluid			
080895-7	600	5.0	20	30	immiscible fluid			
102495-3	650	5.0	20	30	immiscible fluid			
080895-6	700	5.0	20	30	immiscible fluid ?			
111195-4	500	5.0	20	50	immiscible fluid			
111195-2	700	5.0	20	50	immiscible fluid			
111195-6	700	4.0	20	70	immiscible fluid			
111195-3	500	5.0	20	70	immiscible fluid			
111195-7	700	5.0	20	70	immiscible fluid			

Table 1 (continued)

Sample Number	Tf	Pf	Salinity	Mol% CO_2	Th(L-V) (average)	Th(L-V) (range)	n	Method
102093-14	400	2.0	40	5	395 (L)	391 - 398	7	GHFS
041894-4	450	2.0	40	5	434 (L)		1	GHFS
041894-10	450	2.0	40	5	432 (L)	423 - 441	5	GHFS
102093-13	500	2.0	40	5	472 (L)	467 - 476	8	GHFS
102093-10	550	2.0	40	5	509 (L)	506 - 511	12	GHFS
102093-11	600	2.0	40	5.1	575 (L)	574 - 576	7	GHFS
041894-6	625	2.0	40	5	583 (L)	579 - 586	10	GHFS
041894-5	650	2.0	40	5	597 (L)	592 - 601	7	GHFS
041894-7	700	2.0	40	5	625 (L)	617 - 630	7	GHFS
091295-2	400	3.0	40	5	379 (L)	377 - 382	5	GHFS
091295-5	500	3.0	40	5	435 (L)	432 - 437	14	GHFS
091295-7	600	3.0	40	5	481 (L)	475 - 486	25	GHFS
032396-2	700	3.0	40	5	526 (L)	518 - 534	24	GHFS
042796-5	800	3.0	40	5	579 (L)	572 - 587	2	GHFS
070793-8	350	4.0	40	5	343 ? (L)	341 - 345	2	GHFS
041894-8	400	4.0	40	5	372 (L)	363 - 378	8	GHFS
070793-5	450	4.0	40.1	4.9	392 (L)	388 - 393	10	GHFS
081293-8	500	4.0	40	5	411 (L)	408 - 413	11	GHFS
102093-7	550	4.0	40	5	428 (L)	425 - 432	11	GHFS
102093-6	600	4.0	40	5	450 (L)	446 - 452	20	GHFS
102093-9	650	4.0	40	5	476 (L)	474 - 477	12	GHFS
041894-9	650	4.0	40.1	5	472 (L)	470 - 473	12	GHFS
081293-6	700	4.0	40	5	484 (L)	479 - 489	14	GHFS
091295-1	400	5.0	40	5	n.d.			
091295-3	500	5.0	40	5	382 (L)	370 - 392	12	GHFS
032396-1	600	5.0	40	5	413 (L)	408 - 417	20	GHFS
091295-6	700	5.0	40	5	435 (L)	434 - 438	9	GHFS
032396-4	400	3.0	40	10	immiscible fluid			
091295-4	500	3.0	40	10	491 (L) 490 (L)	479 - 500 485 - 495	14 2	GHFS HDAC
032396-6	600	3.0	40	10	592 (L) 579 (L)	588 - 596 574 - 584	16 4	GHFS HDAC
032396-10	700	3.0	40	10	633 (L) 659 (L) 656 (L)	625 - 639 654 - 663 651 - 661	9 7 3	GHFS GHFS HDAC
032396-7	400	4.0	40	10	immiscible fluid			
032396-8	500	4.0	40	10	488 (L)	481 - 495	5	HDAC
042796-4	600	4.0	40	10	575 (L) 556 (L)	571 - 578 546 - 566	3 5	GHFS HDAC
042796-1	700	4.0	40	10	615 (L) 586 (L)	608 - 625 581 - 591	5 2	GHFS HDAC

Table 1 (continued)

Sample Number	Tf	Pf	Salinity	Mol% CO_2	Th(L-V) (average)	Th(L-V) (range)	n	Method
032396-3	400	5.0	40	10	immiscible fluid			
042796-2	500	5.0	40	10	488 (L)	486 - 490	7	HDAC
042796-6	600	5.0	40	10	515 (L)	508 - 522	4	HDAC
042796-3	700	5.0	40	10	559 (L)	549 - 569	7	HDAC
051396-5	500	5.0	40	20	immiscible fluid ?			
032396-5	600	5.0	40	20	568 (L)		1	HDAC
032396-9	700	5.0	40	20	667 (L)	665 - 668	2	HDAC
042796-8	600	6.0	40	20	n.d.			

Table 2: Halite dissolution temperatures in presence of liquid and vapor for synthetic fluid inclusions in the H_2O-NaCl-CO_2 system

Tf = formation temperature (°C); Pf = formation pressure (kbar); Salinity = NaCl concentration of the solution in weight percent relative to H_2O; Mol% CO_2 = carbon dioxide concentration in mol percent relative to H_2O; $Th_{(H+L+V \rightarrow L+V)}$ (average) = average halite dissolution temperature in presence of liquid and vapor (°C); $Th_{(H+L+V \rightarrow L+V)}$ (range) = the range in measured $Th_{(H+L+V \rightarrow L+V)}$ (°C); n = number of measured inclusions; GHFS = gas-flow heating/freezing stage; HDAC = hydrothermal diamond-anvil cell; n.d. = not determined

Sample Number	Tf	Pf	Salinity	Mol% CO_2	$Th_{(H+L+V \rightarrow L+V)}$ (average)	$Th_{(H+L+V \rightarrow L+V)}$ (range)	n	Method
102093-14	400	2.0	40	5	332.4	330.0 - 333.6	8	GHFS
041894-4	450	2.0	40	5	334.1	333.0 - 336.7	9	GHFS
041894-10	450	2.0	40	5	333.8	331.5 - 335.6	11	GHFS
102093-13	500	2.0	40	5	331.5	330.0 - 334.4	11	GHFS
102093-10	550	2.0	40	5	337.6	336.9 - 338.3	10	GHFS
102093-11	600	2.0	40	5.1	338.3	336.6 - 340.0	10	GHFS
041894-6	625	2.0	40	5	337.8	337.1 - 338.7	12	GHFS
041894-5	650	2.0	40	5	337.6	334.4 - 341.5	13	GHFS
041894-7	700	2.0	40	5	339.0	337.0 - 340.3	8	GHFS
091295-2	400	3.0	40	5	331.9	329.6 - 334.1	12	GHFS
091295-5	500	3.0	40	5	333.9	331.6 - 335.1	14	GHFS
091295-7	600	3.0	40	5	336.0	333.0 - 338.0	15	GHFS
032396-2	700	3.0	40	5	333.5	332.2 - 335.8	15	GHFS
042796-5	800	3.0	40	5	335.1	330.6 - 338.8	4	GHFS
070793-8	350	4.0	40	5	≈ 332		1	GHFS
041894-8	400	4.0	40	5	333.7	332.1 - 335.1	6	GHFS
070793-5	450	4.0	40.1	4.9	334.7	333.7 - 336.9	11	GHFS
081293-8	500	4.0	40	5	334.5	333.8 - 335.4	11	GHFS
102093-7	550	4.0	40	5	334.0	332.8 - 334.6	11	GHFS
102093-6	600	4.0	40	5	335.9	334.0 - 337.8	20	GHFS
102093-9	650	4.0	40	5	341.4	340.7 - 342.3	12	GHFS
041894-9	650	4.0	40.1	5	336.6	335.4 - 338.0	11	GHFS
081293-6	700	4.0	40	5	336.4	333.9 - 338.2	14	GHFS
091295-1	400	5.0	40	5	n.d.			
091295-3	500	5.0	40	5	331.8	330.0 - 333.6	11	GHFS
032396-1	600	5.0	40	5	334.8	332.7 - 336.4	16	GHFS
091295-6	700	5.0	40	5	337.8	336.7 - 339.3	18	GHFS
091295-4	500	3.0	40	10	345.4	341.6 - 348.1	22	GHFS
032396-6	600	3.0	40	10	340.9 342.5	337.6 - 344.4 338 - 347	20 8	GHFS HDAC
032396-10	700	3.0	40	10	339.5 342.5	336.5 - 344.3 341 - 343	27 3	GHFS HDAC

Table 2 (continued)

Sample Number	Tf	Pf	Salinity	Mol% CO_2	Th(H+L+V → L+V) (average)	Th(H+L+V → L+V) (range)	n	Method
032396-8	500	4.0	40	10	344.2 344	340.8 - 346.1 343 - 345	20 4	GHFS HDAC
042796-4	600	4.0	40	10	341.6 341.5	340.1 - 343.2 341 - 342	20 2	GHFS HDAC
091295-8	600	4.0	40	10	n.d.			
042796-1	700	4.0	40	10	340.8 341.5	336.2 - 343.3 340 - 343	10 4	GHFS HDAC
042796-2	500	5.0	40	10	340.3 341.5	338.7 - 342.6	15 1	GHFS HDAC
042796-6	600	5.0	40	10	339.4 340	337.0 - 341.0 339 - 341	16 4	GHFS HDAC
042796-3	700	5.0	40	10	342.7 339	334.7 - 346.7	19 1	GHFS HDAC
051396-5	500	5.0	40	20	n.d.			
032396-5	600	5.0	40	20	395		1	HDAC
032396-9	700	5.0	40	20	375	373 - 377	2	HDAC
042796-8	600	6.0	40	20	n.d.			

Table 3. Clathrate melting temperatures in equilibrium with aqueous liquid, liquid CO_2, and vapor CO_2 for synthetic fluid inclusions in the H_2O-NaCl-CO_2 system

Tf = formation temperature (°C); Pf = formation pressure (kbar); Loaded Salinity = NaCl concentration of the loaded standard solution in weight percent relative to H_2O; Mol% CO_2 = carbon dioxide concentration in mol percent relative to H_2O; Tm(CLA) (average) = average clathrate melting temperature in equilibrium with aqueous liquid, liquid CO_2, and vapor CO_2 (°C); Tm(CLA) (range) = the range in measured Tm(CLA) (°C); n = number of measured inclusions; Calculated Salinity = salinity in weight percent relative to H_2O calculated from measured average Tm(CLA) using equation of DIAMOND (1992); n.d. = not determined

Sample Number	Tf	Pf	Loaded Salinity	Mol% CO_2	Tm(CLA) (average)	Tm(CLA) (range)	n	Calculated Salinity
012196-3	400	2.0	6	10	6.9	6.6 - 7.2	5	5.9
012196-4	500	2.0	6	10	7.0	6.7 - 7.2	8	5.7
012196-8	600	2.0	6	10	6.9	6.7 - 7.1	8	5.9
031196-9	650	2.0	6	10	6.8	6.6 - 7.1	11	6.0
031196-10	675	2.0	6	10	6.8	6.6 - 7.0	6	6.0
021896-4	700	2.0	6	10	6.8	6.7 - 7.0	7	6.0
012196-1	400	3.0	6	10	6.9	6.6 - 7.3	11	5.9
012196-2	500	3.0	6	10	6.95	6.7 - 7.1	7	5.8
012196-9	600	3.0	6	10	6.9	6.7 - 7.0	7	5.9
021896-8	700	3.0	6	10	6.8	6.6 - 7.3	8	6.0
050396-5	800	3.0	6	10	6.7	6.5 - 7.0	4	6.2
021896-3	400	4.0	6	10	6.9	6.7 - 7.2	10	5.9
021896-7	500	4.0	6	10	6.9	6.6 - 7.2	10	5.9
031196-3	600	4.0	6	10	6.9	6.7 - 7.2	8	5.9
021896-1	700	4.0	6	10	7.0	6.8 - 7.3	10	5.7
031196-4	700	4.0	6	10	7.0	6.7 - 7.3	9	5.7
012196-5	400	2.0	6	20	6.8	6.6 - 7.0	10	6.0
012196-6	450	2.0	6	20	6.8	6.6 - 7.1	8	6.0
012196-7	500	2.0	6	20	6.9	6.5 - 7.2	10	5.9
040496-1	550	2.0	6	20	6.8	6.6 - 7.2	8	6.0
021896-5	600	2.0	6	20	6.6	6.3 - 7.0	11	6.4
040496-2	650	2.0	6	20	6.7	6.5 - 7.1	6	6.2
031196-1	700	2.0	6	20	6.6	6.2 - 7.0	7	6.4
021896-9	400	3.0	6	20	6.5	6.2 - 6.8	10	6.5
021896-10	500	3.0	6	19.8	6.9	6.6 - 7.2	9	5.9
021896-11	500	3.0	6	20	6.9	6.6 - 7.1	10	5.9
031196-5	600	3.0	6	20	6.8	6.6 - 7.1	10	6.0
040496-3	700	3.0	6	20	6.8	6.6 - 7.1	10	6.0
050396-4	800	3.0	6	20	6.75	6.6 - 7.1	5	6.1
112594-2	450	3.5	10	10	4.5	4.4 - 4.5	3	9.7

Table 3 (continued)

Sample Number	Tf	Pf	Loaded Salinity	Mol% CO_2	Tm(CLA) (average)	Tm(CLA) (range)	n	Calculated Salinity
011895-4	400	2.0	20	10	-4.35	-4.3 - -4.4	3	20.0
031295-5	450	2.0	20	10	-4.4	-4.2 - -4.6	5	20.0
011895-6	500	2.0	20	10	-4.3	-4.2 - -4.4	5	19.9
041395-11	550	2.0	20	10	-4.25	-3.9 - -4.4	6	19.9
011895-1	600	2.0	20	10	-4.35	-4.1 - -4.5	5	20.0
020295-4	650	2.0	20	10	-4.2	-4.0 - -4.4	9	19.8
011895-2	700	2.0	20	10	-4.25	-4.2 - -4.3	6	19.9
041395-10	400	3.0	20	10	-4.35	-4.1 - -4.6	6	20.0
042395-9	450	3.0	20	10	-4.45	-4.1 - -4.9	6	20.1
080895-1	450	3.0	20	10	-4.3	-3.9 - -4.6	9	19.9
042395-7	500	3.0	20	10	-4.3	-4.2 - -4.4	6	19.9
062895-4	500	3.0	20	10	-4.5	-4.2 - -4.8	7	20.1
042395-1	550	3.0	20	10	-4.5	-4.2 - -4.8	9	20.1
041395-6	600	3.0	20	10	-4.1	-3.7 - -4.9	10	19.8
062895-3	600	3.0	20	10	n.d.			
042395-3	650	3.0	20	10	-4.4	-4.2 - -4.6	5	20.0
062895-2	650	3.0	20	10	n.d.			
062895-1	700	3.0	20	9.9	n.d.			
050396-3	800	3.0	20	9.9	-4.2	-3.7 - -4.6	6	19.8
031295-1	400	4.0	20	10	-4.3	-4.2 - -4.4	6	19.9
031295-4	450	4.0	20	10	-4.3	-4.1 - -4.5	6	19.9
011895-8	500	4.0	20	10	-4.2	-4.2 - -4.3	5	19.8
041395-7	550	4.0	20	10	-4.1	-3.9 - -4.3	10	19.8
031295-2	600	4.0	20	10	-4.5	-4.3 - -4.6	7	20.1
031295-3	650	4.0	20	10	-4.2	-4.1 - -4.5	6	19.8
020295-5	700	4.0	20	10	-4.2	-4.0 - -4.4	9	19.8
040496-5	800	4.0	20	9.9	-4.6	-4.3 - -4.9	6	20.2
042395-2	400	5.0	20	10	-4.4	-4.1 - -4.7	10	20.0
042395-8	450	5.0	20	10	-4.2	-4.1 - -4.3	7	19.8
042395-5	500	5.0	20	10	-4.3	-4.1 - -4.7	9	19.9
042395-4	550	5.0	20	9.9	-4.25	-4.0 - -4.4	6	19.9
042395-6	600	5.0	20	10	-4.3	-4.1 - -4.4	8	19.9
062895-5	650	5.0	20	10	-4.35	-4.0 - -4.9	13	20.0
062895-6	700	5.0	20	10	-4.3	-4.0 - -4.5	10	19.9
020295-8	400	2.0	20	20	n.d.			
022695-1	450	2.0	20	20.1	n.d.			
020295-7	500	2.0	20	20.1	n.d.			
022695-4	600	2.0	20	20	n.d.			
022695-3	650	2.0	20	19.9	n.d.			
022695-2	700	2.0	20	20.1	n.d.			

Table 3 (continued)

Sample Number	Tf	Pf	Loaded Salinity	Mol% CO_2	Tm(CLA) (average)	Tm(CLA) (range)	n	Calculated Salinity
032595-3	400	3.0	20	20		-4.1 - -6.9	3	19.8 - 22.0
051595-4	450	3.0	20	20		-5.8 - -7.4	9	21.2 - 22.4
051595-3	500	3.0	20	20	-4.7	-4.3 - -4.9	10	20.3
071195-4	550	3.0	20	19.9	-4.85	-4.1 - -5.8	7	20.4
032595-2	600	3.0	20	20	-4.3	-4.1 - -4.5	5	19.9
060695-6	650	3.0	20	20	-4.25	-3.8 - -4.8	14	19.9
032595-4	700	3.0	20	20	-4.2	-3.5 - -4.4	9	19.8
060695-2	400	4.0	20	20		-5.9 - -6.8	5	21.3 - 22.0
060695-1	450	4.0	20	20		-4.7 - -6.8	8	20.3 - 22.0
060695-3	500	4.0	20	20	-4.35	-4.0 - -4.8	11	20.0
111195-5	550	4.0	20	20	-4.25	-4.0 - -4.5	10	19.9
031295-7	600	4.0	20	20	-4.4	-3.9 - -4.8	9	20.0
060695-4	650	4.0	20	20	-4.4	-4.1 - -4.6	9	20.0
031295-6	700	4.0	20	20	-4.7	-4.5 - -4.9	6	20.3
071195-1	400	5.0	20	20		-5.5 - -5.6	4	20.9 -21.0
071195-2	450	5.0	20	19.9	-4.6	-4.3 - -4.9	8	20.2
060695-5	500	5.0	20	20	-4.3	-4.2 - -4.4	7	19.9
071195-3	550	5.0	20	20	-4.4	-4.1 - -4.6	9	20.0
051595-2	600	5.0	20	20.1	-4.4	-4.1 - -4.8	8	20.0
062895-7	700	5.0	20	20	-4.25	-3.8 - -4.6	9	19.9
062895-8	500	3.0	20	29.9	n.d., most inclusions contain halite			
080895-3	400	4.0	20	29.9		-4.5 - -9.9	5	20.1->23.2
102495-4	500	4.0	20	30	n.d., many inclusions contain halite			
071195-5	600	4.0	20	29.9	n.d., many inclusions contain halite			
080895-8	700	4.0	20	30	n.d., many inclusions contain halite			
080895-2	400	5.0	20	29.9	n.d.			
102495-2	450	5.0	20	29.9	n.d.			
080895-5	500	5.0	20	30	n.d., many inclusions contain halite			
102495-1	550	5.0	20	30		-8.5 - -9.9	4	≥ 23.2
080895-7	600	5.0	20	30		-4.4 - -6.8	11	20.0 - 22.0
102495-3	650	5.0	20	30	n.d.			
080895-6	700	5.0	20	30	-4.95	-3.2 - -6.9	13	20.5
111195-4	500	5.0	20	50	n.d., many inclusions contain halite			
111195-2	700	5.0	20	50	n.d., many inclusions contain halite			
111195-6	700	4.0	20	70	n.d., many inclusions contain halite			
111195-3	500	5.0	20	70	n.d., many inclusions contain halite			
111195-7	700	5.0	20	70	n.d., many inclusions contain halite			

Table 4. Density of the CO_2-rich phase for synthetic fluid inclusions in the H_2O-NaCl-CO_2 system

Tf = formation temperature (°C); Pf = formation pressure (kbar); Salinity = NaCl concentration of the solution in weight percent relative to H_2O; Mol% CO_2 = carbon dioxide concentration in mol percent relative to H_2O; Th(CO_2) = homogenization temperature of the CO_2-rich phases (°C); (L/A) = homogenization to the liquid CO_2 phase, average of the measured Th(CO_2); (V/M) = homogenization to the vapor CO_2 phase, maximum of the measured Th(CO_2); d(CO_2) = density of the CO_2-rich phase (g/cm^3); (MT) = density of the CO_2-rich phase determined microthermometrically from Th(CO_2); (RS) = density of the CO_2-rich phase determined at 32 °C using Raman spectroscopy ; d(CO_2) (range) = the range in measured d(CO_2) (g/cm^3); n = number of measured inclusions; n.d. = not determined

Sample Number	Tf	Pf	Salinity	Mol% CO_2	Th(CO_2)	d(CO_2)	d(CO_2) (range)	n
012196-3	400	2.0	6	10	30.45 (V/M)	0.361 (MT)		10
012196-4	500	2.0	6	10	28.2 (V/M)	0.287 (MT)		14
012196-8	600	2.0	6	10	22.9 (V/M)	0.215 (MT)		12
031196-9	650	2.0	6	10	17.9 (V/M)	0.176 (MT)		8
031196-10	675	2.0	6	10	17.2 (V/M)	0.172 (MT)		9
021896-4	700	2.0	6	10	15.0 (V/M)	0.159 (MT)		8
012196-1	400	3.0	6	10	28.58 (L/A)	0.649 (MT)	0.643 - 0.653	30
012196-2	500	3.0	6	10	30.2 (V/M)	0.347 (MT)		15
012196-9	600	3.0	6	10	28.5 (V/M)	0.293 (MT)		12
021896-8	700	3.0	6	10	24.8 (V/M)	0.235 (MT)		16
050396-5	800	3.0	6	10	19.5 (V/M)	0.187 (MT)		7
021896-3	400	4.0	6	10	24.09 (L/A)	0.729 (MT)	0.704 - 0.750	30
021896-7	500	4.0	6	10	29.51 (L/A)	0.621 (MT)	0.618 - 0.625	30
031196-3	600	4.0	6	10	30.3 (V/M)	0.352 (MT)		14
021896-1	700	4.0	6	10	29.5 (V/M)	0.320 (MT)		16
031196-4	700	4.0	6	10	28.8 (V/M)	0.300 (MT)		16
012196-5	400	2.0	6	20	29.63 (L/A)	0.617 (MT)	0.610 - 0.628	32
012196-6	450	2.0	6	20	30.67 (L/A)	0.560 (MT)	0.546 - 0.592	33
012196-7	500	2.0	6	20	30.65 (V/M)	0.376 (MT)		19
040496-1	550	2.0	6	20	30.4 (V/M)	0.358 (MT)		15
021896-5	600	2.0	6	20	30.1 (V/M)	0.342 (MT)		16
040496-2	650	2.0	6	20	29.2 (V/M)	0.311 (MT)		10
031196-1	700	2.0	6	20	28.1 (V/M)	0.284 (MT)		12
021896-9	400	3.0	6	20	23.54 (L/A)	0.737 (MT)	0.702 - 0.784	36
021896-10	500	3.0	6	19.8	29.31 (L/A)	0.628 (MT)	0.621 - 0.634	30
021896-11	500	3.0	6	20	29.1 (L/A)	0.634 (MT)	0.631 - 0.637	30
031196-5	600	3.0	6	20	29.96 (L/A)	0.603 (MT)	0.602 - 0.606	30
040496-3	700	3.0	6	20	30.7 (V/M)	0.381 (MT)		15
050396-4	800	3.0	6	20	29.7 (V/M)	0.326 (MT)		5
112594-2	450	3.5	10	10	29.87 (L/A)	0.607 (MT)	0.601 - 0.611	13

Table 4 (continued)

Sample Number	Tf	Pf	Salinity	Mol% CO_2	Th(CO_2)	d(CO_2)	d(CO_2) (range)	n
011895-4	400	2.0	20	10	30.2 (L/A)	0.592 (MT)		3
031295-5	450	2.0	20	10	29.4 (V/M)	0.316 (MT)		7
011895-6	500	2.0	20	10	28.9 (V/M)	0.302 (MT)		12
041395-11	550	2.0	20	10	28.5 (V/M)	0.293 (MT)		12
011895-1	600	2.0	20	10	27.7 (V/M)	0.277 (MT)		15
020295-4	650	2.0	20	10	23.7 (V/M)	0.223 (MT)		8
011895-2	700	2.0	20	10	22.9 (V/M)	0.215 (MT)		12
041395-10	400	3.0	20	10	28.49 (L/A)	0.651 (MT)	0.634 - 0.660	17
042395-9	450	3.0	20	10	29.83 (L/A)	0.609 (MT)	0.597 - 0.628	19
080895-1	450	3.0	20	10	30.09 (L/A)	0.597 (MT)	0.592 - 0.602	20
042395-7	500	3.0	20	10	29.77 (L/A)	0.611 (MT)	0.610 - 0.614	16
062895-4	500	3.0	20	10	29.8 (V/M)	0.330 (MT)		13
042395-1	550	3.0	20	10	30.1 (V/M)	0.342 (MT)		12
041395-6	600	3.0	20	10	29.6 (V/M)	0.323 (MT)		11
062895-3	600	3.0	20	10	n.d.			
042395-3	650	3.0	20	10	29.0 (V/M)	0.305 (MT)		7
062895-2	650	3.0	20	10	n.d.			
062895-1	700	3.0	20	9.9	n.d.			
050396-3	800	3.0	20	9.9	21.4 (V/M)	0.202 (MT)		5
031295-1	400	4.0	20	10	22.71 (L/A)	0.747 (MT)	0.721 - 0.775	25
031295-4	450	4.0	20	10	27.39 (L/A)	0.676 (MT)	0.651 - 0.691	15
011895-8	500	4.0	20	10	29.36 (L/A)	0.626 (MT)	0.621 - 0.631	16
041395-7	550	4.0	20	10	29.98 (L/A)	0.602 (MT)	0.597 - 0.606	17
031295-2	600	4.0	20	10	30.2 (V/M)	0.347 (MT)		10
031295-3	650	4.0	20	10	30.1 (V/M)	0.342 (MT)		11
020295-5	700	4.0	20	10	29.8 (V/M)	0.330 (MT)		9
040496-5	800	4.0	20	9.9	29.1 (V/M)	0.308 (MT)		7
042395-2	400	5.0	20	10	12.66 (L/A)	0.842 (MT)	0.816 - 0.884	33
042395-8	450	5.0	20	10	20.4 (L/A)	0.773 (MT)	0.758 - 0.783	28
042395-5	500	5.0	20	10	25.73 (L/A)	0.705 (MT)	0.698 - 0.714	18
042395-4	550	5.0	20	9.9	28.72 (L/A)	0.645 (MT)	0.643 - 0.648	17
042395-6	600	5.0	20	10	29.67 (L/A)	0.615 (MT)	0.610 - 0.621	18
062895-5	650	5.0	20	10	29.9 (L/A)	0.606 (MT)	0.601 - 0.610	21
062895-6	700	5.0	20	10	30.9 (V/M)	0.407 (MT)		14
032595-3	400	3.0	20	20	28.05 (L/A)	0.662 (MT)	0.643 - 0.674	14
051595-4	450	3.0	20	20	27.76 (L/A)	0.668 (MT)	0.618 - 0.792	17
051595-3	500	3.0	20	20	28.0 (L/A)	0.663 (MT)	0.658 - 0.667	21
071195-4	550	3.0	20	19.9	29.63 (L/A)	0.617 (MT)	0.614 - 0.621	15
032595-2	600	3.0	20	20	29.9 (L/A)	0.606 (MT)	0.604 - 0.606	10
060695-6	650	3.0	20	20	30.13 (L/A)	0.595 (MT)	0.586 - 0.602	25
032595-4	700	3.0	20	20	30.6 (V/M)	0.372 (MT)		13

Table 4 (continued)

Sample Number	Tf	Pf	Salinity	Mol% CO_2	Th(CO_2)	d(CO_2)	d(CO_2) (range)	n
060695-2	400	4.0	20	20	20.4 (L/A)	0.762 (MT)	0.738 - 0.800	15
060695-1	450	4.0	20	20	19.97 (L/A)	0.778 (MT)	0.742 - 0.788	25
060695-3	500	4.0	20	20	21.99 (L/A)	0.756 (MT)	0.750 - 0.759	27
111195-5	550	4.0	20	20	24.96 (L/A)	0.717 (MT)	0.712 - 0.721	40
031295-7	600	4.0	20	20	27.86 (L/A)	0.666 (MT) 0.588 (RS)	0.658 - 0.669 0.567 - 0.619	14 9
060695-4	650	4.0	20	20	28.44 (L/A)	0.652 (MT)	0.646 - 0.656	20
031295-6	700	4.0	20	20	29.38 (L/A)	0.625 (MT)	0.621 - 0.628	14
071195-1	400	5.0	20	20	4.31 (L/A)	0.901 (MT)	0.881 - 0.945	19
071195-2	450	5.0	20	19.9	7.58 (L/A)	0.879 (MT)	0.840 - 0.933	40
060695-5	500	5.0	20	20	12.72 (L/A)	0.842 (MT)	0.834 - 0.849	20
071195-3	550	5.0	20	20	17.93 (L/A)	0.798 (MT)	0.794 - 0.803	30
051595-2	600	5.0	20	20.1	21.59 (L/A)	0.760 (MT)	0.756 - 0.763	20
062895-7	700	5.0	20	20	27.06 (L/A)	0.682 (MT)	0.678 - 0.689	28
080895-5	500	5.0	20	30	16.7-17.5(L)	(MT)	0.802 - 0.809	3
102495-1	550	5.0	20	30	10.3-16.3(L)	(MT)	0.812 - 0.860	6
080895-7	600	5.0	20	30	15.66 (L/A)	0.818 (MT)	0.798 - 0.830	26
080895-6	700	5.0	20	30	21.48 (L/A)	0.762 (MT)	0.755 - 0.766	30
102093-14	400	2.0	40	5	27.4 (V/M)	0.271 (MT)		4
041894-4	450	2.0	40	5	24.8 (V/M)	0.235 (MT) 0.292 (RS)	 0.269 - 0.321	6 6
041894-10	450	2.0	40	5	22.1 (V/M)	0.208 (MT)		5
102093-13	500	2.0	40	5	23.8 (V/M)	0.224 (MT) 0.248 (RS)	 0.225 - 0.273	11 4
102093-10	550	2.0	40	5	22.0 (V/M)	0.207 (MT) 0.230 (RS)	 0.213 - 0.261	13 6
102093-11	600	2.0	40	5.1	16.4 (V/M)	0.167 (MT) 0.213 (RS)	 0.185 - 0.233	11 10
041894-6	625	2.0	40	5	15.7 (V/M)	0.163 (MT) 0.200 (RS)	 0.181 - 0.229	8 9
041894-5	650	2.0	40	5	15.5 (V/M)	0.162 (MT)		9
041894-7	700	2.0	40	5	14.2 (V/M)	0.155 (MT) 0.178 (RS)	 0.137 - 0.221	14 4
091295-2	400	3.0	40	5	28.4 (V/M)	0.291 (MT)		7
091295-5	500	3.0	40	5	27.9 (V/M)	0.281 (MT)		12
091295-7	600	3.0	40	5	25.2 (V/M)	0.240 (MT)		15
032396-2	700	3.0	40	5	18.4 (V/M)	0.180 (MT)		8
042796-5	800	3.0	40	5	2.9 (V/M)	0.108 (MT)		3

Table 4 (continued)

Sample Number	Tf	Pf	Salinity	Mol% CO_2	Th(CO_2)	d(CO_2)	d(CO_2) (range)	n
070793-8	350	4.0	40	5	29.1 (L/A)	0.634 (MT) 0.62 ? (RS)	0.628 - 0.640	3 1
070793-5	450	4.0	40.1	4.9	29.8 (V/M)	0.330 (MT) 0.409 (RS)	0.394 - 0.418	9 4
081293-8	500	4.0	40	5	28.7 (V/M)	0.298 (MT) 0.368 (RS)	0.341 - 0.402	11 20
102093-7	550	4.0	40	5	28.3 (V/M)	0.289 (MT) 0.325 (RS)	0.289 - 0.349	10 10
102093-6	600	4.0	40	5	26.6 (V/M)	0.259 (MT) 0.274 (RS)	0.265 - 0.277	11 4
102093-9	650	4.0	40	5	24.3 (V/M)	0.230 (MT) 0.237 (RS)	0.232 - 0.241	11 3
041894-9	650	4.0	40.1	5	24.4 (V/M)	0.231 (MT)		9
081293-6	700	4.0	40	5	24.3 (V/M)	0.230 (MT) 0.218 (RS)	0.197 - 0.241	24 6
091295-1	400	5.0	40	5	28.0 (L/A)	0.663 (MT)	0.651 - 0.678	11
091295-3	500	5.0	40	5	29.3 (V/M)	0.314 (MT)		12
032396-1	600	5.0	40	5	29.9 (V/M)	0.334 (MT)		6
091295-6	700	5.0	40	5	23.8 (V/M)	0.224 (MT)		7
032396-4	400	3.0	40	10	29.8 (V/M)	0.330 (MT)		9
091295-4	500	3.0	40	10	30.4 (V/M)	0.358 (MT)		18
032396-6	600	3.0	40	10	29.8 (V/M)	0.330 (MT)		10
032396-10	700	3.0	40	10	28.9 (V/M)	0.302 (MT)		4
032396-7	400	4.0	40	10	29.01 (L/A)	0.637 (MT)	0.610 - 0.692	9
032396-8	500	4.0	40	10	29.36 (L/A)	0.626 (MT)	0.614 - 0.631	39
091295-8	600	4.0	40	10	29.49 (L/A)	0.622 (MT)	0.618 - 0.634	30
042796-4	600	4.0	40	10	29.22 (L/A)	0.631 (MT)	0.625 - 0.637	25
042796-1	700	4.0	40	10	29.9 (V/M)	0.334 (MT)		7
032396-3	400	5.0	40	10	27.27 (L/A)	0.677 (MT)	0.621 - 0.738	27
042796-2	500	5.0	40	10	27.8 (L/A)	0.667 (MT)	0.606 - 0.696	22
042796-6	600	5.0	40	10	29.8 (L/A)	0.610 (MT)	0.597 - 0.625	27
042796-3	700	5.0	40	10	29.99 (L/A)	0.601 (MT)	0.597 - 0.606	25
051396-5	500	5.0	40	20	27.82 (L/A)	0.667 (MT)	0.631 - 0.683	33
032396-5	600	5.0	40	20	29.26 (L/A)	0.629 (MT)	0.610 - 0.643	57
032396-9	700	5.0	40	20	29.43 (L/A)	0.627 (MT)	0.610 - 0.634	34
042796-8	600	6.0	40	20	24.97 (L/A)	0.717 (MT)	0.692 - 0.738	32

Table 5: Regression coefficients (A, B) for linear equations (Tf = A*Th + B) along isobars of formation pressure (Pf) relating homogenization temperature (Th) and formation temperature (Tf) of synthetic fluid inclusions in the H_2O-NaCl-CO_2 system

Th = homogenization temperature (°C); Tf = formation temperature (°C); Pf = formation pressure (kbar); Wt% NaCl = NaCl concentration of the solution in weight percent relative to H_2O; Mol% CO_2 = carbon dioxide concentration in mol percent relative to H_2O

Wt% NaCl	Mol% CO_2	Pf (kbar)	A	B	Valid Th Range (°C)
6	10	2	3.0598	-508.93	290 - 400
6	10	3	4.3281	-812.7	275 - 400
6	10	4	6.1721	-1265.47	275 - 350...400
6	20	2	1.4686	-17.81	(325)...350 - 500
6	20	3	3.4254	-605.15	(325)...350 - 500
20	10	2	1.359	-84.99	400 - 600
20	10	3	2.7996	-606.19	360 - 600
20	10	4	3.867	-958.02	360 - 450...550
20	10	5	5.3051	-1416.3	360 - 400
20	20	3	1.5501	-243.26	475 - 625
20	20	4	2.5478	-675.8	460 - 625
20	20	5	4	-1320	460 - 500
40	5	2	1.2504	-91.91	(380)...400 - 625
40	5	3	2.0336	-376.14	(380)...400 - 625
40	5	4	2.5411	-544.46	(380)...400 - 550
40	5	5	3.7377	-932.44	(380 - 450)
40	10	3	1.2027	-91.57	500 - 650
40	10	4	1.9434	-455.92	500 - 650
40	10	5	2.7641	-839.16	500 - 525...(575)

VITA

Christian Schmidt was born on April 14th, 1964 in Berlin, Germany. From 1980-1983, he had a mining apprenticeship at the SDAG Wismut, Thuringia, Germany, and worked as a miner until 1985. He received his Diploma (M.S.) in Geology from the Bergakademie Freiberg, Saxony, Germany, in 1990. Following two years as an assistant at the Department of Geosciences at the Bergakademie Freiberg, he enrolled in graduate school at Virginia Tech and completed his Ph.D. in geology in 1997. He currently plans to return to Germany for a postdoctoral position in experimental petrology at the Geoforschungszentrum (Geosciences Research Center) Potsdam.

_____

Christian Schmidt